THE JOURNAL OF PHYSICAL CHEMISTRY B

Article

Cite This: J. Phys. Chem. B XXXX, XXX, XXX–XXX

pubs.acs.org/JPCB

Simple and Efficient Theoretical Approach To Compute 2D Optical Spectra

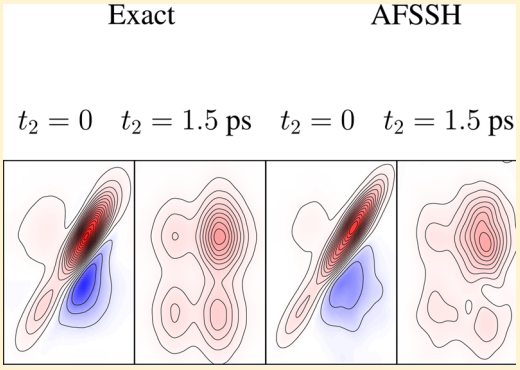
Amber Jain,*,† Andrew S. Petit,‡ Jessica M. Anna,§ and Joseph E. Subotnik*,§

†Department of Chemistry, Indian Institute of Technology Bombay, Mumbai, 400076, India

‡Department of Chemistry and Biochemistry, California State University, Fullerton, California 92834, United States

§Department of Chemistry, University of Pennsylvania, 231 South 34th Street, Philadelphia, Pennsylvania 19104, United States

ABSTRACT: A highly efficient scheme is proposed and benchmarked to compute 2D optical spectra. This scheme is ideally designed for electronic spectroscopy; however, the method can be applied in a straightforward way to vibrational spectroscopy as well. Our scheme performs dynamics only for the t_2 duration, eliminating explicit t_1 and t_3 coherent dynamics and thus can achieve dramatic improvements in efficiency. To gain this efficiency, we assume the system is in the inhomogeneous regime and that there is no significant nonadiabatic transfer of population during the t_1 and t_3 coherence times. Preliminary results are presented for the Frenkel Hamiltonian. We obtain excellent agreement with numerically exact results (which are possible for this simplistic model Hamiltonian), capturing all relevant trends at least qualitatively (and sometimes quantitatively).



Downloaded via UNIV OF PENNSYLVANIA on February 13, 2019 at 14:46:20 (UTC).
See https://pubs.acs.org/sharingguidelines for options on how to legitimately share published articles.

1. INTRODUCTION

Over the past two decades, the area of two-dimensional optical spectroscopy has emerged as an important tool for investigating condensed phase systems.[1−8] 2D optical spectroscopy is a third-order nonlinear spectroscopy where three incoming laser pulses interact with a molecule or material, inducing a third-order polarization that leads to the emission of a signal. 2D spectroscopy is similar to pump−probe spectroscopy but spreads the information contained in a pump−probe spectrum over two frequency axes. The signal is detected through spectral interferometry, enabling both high frequency and high temporal resolution to be maintained. By spreading the information over two frequency axes, one can distinguish between homogeneous and inhomogeneous broadening[9] and better interpret congested signals. A schematic of the pulse sequence used to obtain a 2D spectrum is shown in Figure 1, and 2D spectroscopies in different spectral regions, including 2D-IR,[10] 2DES,[4] 2DEV, and 2DVE,[11] have been applied to study a variety of systems.[7,8] One of the main challenges in using multidimensional techniques is in interpreting congested spectra, where theoretical simulations may be required. Moreover, simulating 2D spectra of complex systems can be very arduous, such that one cannot always rely on theory or computation to help interpret a congested signal.

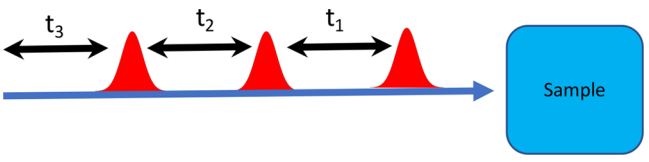


Figure 1. Schematic of a 2D pulse sequence. A sample is interrogated by three laser pulses. The usual two-dimensional visualization (as in Figure 7) is usually presented for a fixed t_2 "waiting time" after Fourier transforming over the first coherence time t_1 and the second coherence time t_3. By requiring a grid in multiple dimensions of time, calculations can be very demanding.

To understand why multidimensional spectroscopy is so difficult to simulate, recall the usual framework for understanding the spectra of molecules in solution (which dates back to Kubo[12,13]) and consider the hierarchy of approaches available. For a two-level system ($|g\rangle$, $|e\rangle$) interacting with its environment, assuming the dipole moment is of the form $\hat{\mu} = \mu_{ge}\ |g\rangle\langle e| + |e\rangle\langle g|$, the absorption spectrum can be calculated with linear response as follows:

Level A:

$$I(\omega) \propto \int_{-\infty}^{\infty} dt\ e^{i\omega t}\langle \hat{\mu}(t)\,\hat{\mu}(0)\rangle = \int_{-\infty}^{\infty} dt\ e^{i\omega t}\langle e^{i\hat{H}_g t/\hbar}\hat{\mu}e^{-i\hat{H}_e t/\hbar}\hat{\mu}\rangle \quad (1)$$

Here, in order to calculate the absorption spectrum in the frequency domain, we are required to propagate dynamics on both the excited and ground state surfaces (with Hamiltonians $\hat{H}_g$ and $\hat{H}_e$). As derived by Kubo,[9] assuming the Condon approximation, the simplest means to evaluate this response function is through a transformation to the interaction picture, whereby one must evaluate the energy gap correlation function:

Received: September 5, 2018
Revised: December 9, 2018

© XXXX American Chemical Society

DOI: 10.1021/acs.jpcb.8b08674
J. Phys. Chem. B XXXX, XXX, XXX–XXX

Level B:

$$I(\omega) \propto |\mu_{ge}|^2 \int_{-\infty}^{\infty} dt\ e^{i\omega t} \left\langle \exp\left(\int_0^t \frac{-i}{\hbar} \hat{\Omega}_{eg}(t')\ dt' \right) \right\rangle \quad (2)$$

$\hat{\Omega}_{eg}$ is defined as the energy gap, $\hat{\Omega}_{eg} = \hat{H}_e - \hat{H}_g$. Equation 2 is formally exact if all dynamics are performed quantum mechanically with a time-ordered exponential.[9] In practice, one usually evaluates the energy gap classically or semiclassically,[14] which leads to some ambiguity as to the surface of propagation in eq 2.[15] The usual approach is to run classical dynamics either on the ground state or on an excited state,[16] or even better, on the average of the two states.[17,18] Obviously, this problem becomes more acute for electronic spectroscopies, because electronic potential energy surfaces are far from parallel, and semiclassical schemes to calculate linear absorption and nonlinear transient absorption spectra must be designed appropriately.[19−23] Nevertheless, even with classical propagation, level B captures all of the salient features of linear electronic spectroscopy, including asymmetric line shapes, motional narrowing and inhomogeneous broadening.

If one further invokes a cumulant expansion, one reduces the absorption spectrum to an integral over the frequency−frequency correlation function.[16]

Level C:

$$I(\omega) \propto |\mu_{ge}|^2 \int_{-\infty}^{\infty} dt e^{i\omega t} \exp\left(- \int_0^t d\tau' \int_0^{\tau'} d\tau'' \langle \Omega_{eg}(\tau') \Omega_{eg}(\tau'') \rangle \right) \quad (3)$$

Here, if one evaluates the correlation function classically, one again faces the problem of how exactly to run the dynamics (i.e., along which surface). Nevertheless, even at this level of approximation, one still captures some key features (e.g., the distinction between inhomogeneous broadening and motional narrowing) with minimal cost. Furthermore, for harmonic potentials, one can evaluate the correlation function quantum mechanically which captures the asymmetry of the absorption spectrum.

Finally, the very simplest approach is just to make a histogram of the excitation energies, which represents just the "inhomogeneous" spectrum:

Level D:

$$I(\omega) \propto |\mu_{ge}|^2 \langle \delta(\hat{\Omega}_{eg} - \hbar\omega) \rangle \quad (4)$$

With all of the tools above, one can usually find a balance between computational cost and accuracy. For expensive *ab initio* or semiempirical calculations, one must usually stick with level D (or maybe C);[24] in most situations, there is at least one approach available (even if painful).

Unfortunately, however, for 2D spectroscopy, the physics is more complicated. First, because there are formally three times of interest, t_1, t_2, and t_3, and because the standard practice is to Fourier transform over the first and third dynamical time periods, the number of trajectories (of different lengths) that must be performed can be enormous: for every grid point (t_1, t_3), one should run multiple trajectories; see Figure 1. Second, wavepackets are launched on ground and excited state surfaces (rather than the ground state only) and dynamics can occur over long t_2 waiting times, which dramatically increases computational demands. Third, especially for 2DES spectra, the excited state potential energy surfaces can intersect and can have very different character, such that one requires techniques for modeling nonadiabatic dynamics explicitly.[25]

As a consequence of these differences, there is a limited hierarchy of approaches available for modeling 2D optical spectra; in particular, there are few very cheap techniques that can be combined with expensive *ab initio* electronic structure.[26] To address this obstacle, several groups are now developing algorithms to simulate 2D spectra. The most rigorous approach (i.e., level A) is to work with a model Hamiltonian of a few quantum levels coupled to harmonic baths and then solve for the 2D spectra exactly with numerically exact methods such as quasi-adiabatic path integrals (QUAPI)[27−29] or the hierarchical equations of motion (HEOM).[30,31] In this work, we have used the HEOM method for computing numerically exact results. See section 3.2 below.

Beyond exact HEOM calculations, a level B calculation would be to expand all propagators as integrals over energy gaps $\hat{\Omega}_{ij} = \hat{H}_i - \hat{H}_j$ as above in eq 2. In practice, however, this technique is rarely applied for 2DES spectroscopy—where there are multiple nonparallel surfaces and excited state dynamics are important—and one can no longer ignore exactly how the nuclear dynamics are calculated in eq 2: which surface enters at which time? This point is highlighted in ref 32, where a few different approaches are compared. In the end, even though level B calculations have been very successful for 2D-IR[33] (especially if one maps electronic energies to electric fields[34]), for 2DES the presence of many nonparallel electronic states and the need for three independent propagation times makes these calculations far more difficult, and given the need to converge phases, *ab initio* calculations become intractable.

Thus, for 2D spectra, the usual approach is a level C methodology, whereby one performs a cumulant expansion and then expresses the line shape in terms of the set of energy gap correlation functions between all states, $\{\langle \hat{\Omega}_{ij} \hat{\Omega}_{kl}(t) \rangle\}$.[10,35,36] This approach is extremely efficient and works very well for 2D-IR,[37] and yet these results are not robust for 2DES with large t_2 waiting times: for an analytic approximation of the line shapes with cumulants, one must ignore the diabatic couplings between electronic states. In other words, in general, these approaches assume that the solvent couples directly to the adiabatic electronic states and thus one ignores all nonadiabatic dynamics (e.g., associated with electron transfer).[35,36] Furthermore, for harmonic surfaces, correlation functions can be calculated analytically, but no such simplification is possible beyond harmonic surfaces.

With this in mind, many researchers are currently seeking to go beyond the cumulant expansion for modeling 2D-ES spectra, looking for tractable means to evaluate spectra while including excited state dynamics. In general, the essential question is how does one calculate multitime correlation functions in a reasonable amount of time? For instance, recently, Loring has suggested an optimized mean-field trajectory (OMT) approach[38] for calculating spectra based on the Meyer−Miller mapping of quantum variables to classical variables.[39,40] Although to our knowledge the OMT technique has so far only generated $t_2 > 0$ spectra for 2D-IR,[41] the approach should be in principle generalizable to $t_2 > 0$ 2DES spectra.[38] Concurrently, Coker et al. have recently developed a path integral approach based on partially linearized dynamics and have demonstrated impressive results.[42] From a different perspective, Jansen and co-workers

DOI: 10.1021/acs.jpcb.8b08674
J. Phys. Chem. B XXXX, XXX, XXX−XXX

have suggested propagating either Ehrenfest or surface hopping dynamics over the t_1, t_2, t_3 time periods to fully evaluate the three-time response functions, from which one can easily extract spectra. These approaches have proven able to reproduce several of the key features found in HEOM spectra.[43,44] Furthermore, recent work by Tempelaar and Reichman[45] has suggested further improvements to these surface hopping approaches, whereby one temporarily propagates extra trajectories in order to calculate an off-diagonal correlation function. Altogether, refs 38, 42, 43, 44, and 45 show great promise for extracting 2DES signals. And yet, even for these methods, it is still not clear that these methods will easily allow for *ab initio* calculations, given the need for three-time correlation functions (see eq 17 below), which are expensive.

In the present paper, we seek to build upon the work of Jansen's group[44] and ask a very naive question: if we restrict ourselves (a) to the inhomogeneous regime and assume (b) no significant nonadiabatic transfer of population during the t_1 and t_3 coherence times as well as (c) a reasonably high temperature of the bath, can we construct a simple algorithm for 2D spectra *without building up the full three-time correlation function?* In particular, can we extract a rough 2D spectra from a dynamics calculation propagated only during the t_2 waiting time (and not t_1 or t_3)? If we can achieve such a simplification, the cost of simulating 2D spectra would be reduced dramatically. Below, we will argue that such a simplification is possible within the confines of the three conditions listed above. Effectively, as detailed below, our ansatz is that an approximate 2D spectrum can obtained by following the instantaneous energy gap during the t_2 waiting time, and then broadening the resulting energy map to align with a cumulant expansion. Importantly, the three necessary assumptions listed above (that underlie our method) should be valid for many experimental conditions commonly used in condensed phase 2D-ES spectroscopy with polar or hydrogen-bonding solvents.

As far as analyzing our simulated 2D spectra, we will pay close attention to two details that reflect the intrinsic system dynamics: (a) Do we capture the correct nonadiabatic transfer of intensity from diagonal peaks to off-diagonal peaks, corresponding to the correct rate of electronic relaxation, i.e., excited state dynamics? And (b), do we recover the correct homogeneous broadening of the peaks? We will show below that these features can indeed be recovered, sometimes nearly quantitatively.

An outline of this paper is as follows: In section 2, we describe the standard, harmonic model Hamiltonian for benchmarking 2D spectra calculations. In section 3, we review both the standard theoretical descriptions of 2D spectra, along with the HEOM approach; thereafter, we offer a new, streamlined surface hopping approach which will be tested. In section 4, we discuss our results. We conclude in section 5 and hypothesize about the utility of the present method.

2. MODEL HAMILTONIAN AND NOTATION

For this paper, only so that we may compare with exact dynamics, the Hamiltonian for the molecular system is chosen to be of a Frenkel form with M two-level systems:

$$H_{\mathrm{mol}} = H_{\mathrm{el}} + H_{\mathrm{b}} + H_{\mathrm{eb}} \tag{5}$$

Here and henceforward, we will drop the hat notation for operators and, e.g., write H_{el} in place of $\hat{H}_{\mathrm{el}}$. H_{el} denotes the electronic Hamiltonian for linearly coupled two-level systems:

$$H_{\mathrm{el}} = \sum_{i=1}^{M} \epsilon_i d_i^\dagger d_i + \sum_{i<j}^{M} V_{ij}^{\mathrm{c}} (d_i d_j^\dagger + d_j d_i^\dagger) \tag{6}$$

d_i ($d_i^\dagger$) is the annihilation (creation) operator for molecule i and V^{c} is the diabatic coupling. The bath Hamiltonian H_{b} is composed of M independent sets of harmonic oscillators with Hamiltonian given by

$$H_{\mathrm{b}} = \sum_{i=1}^{M} \sum_{\alpha=1}^{N} \left(\frac{{p_{i\alpha}}^2}{2m} + \frac{1}{2} m {\omega_{i\alpha}}^2 {R_{i\alpha}}^2 \right) \tag{7}$$

We define N to be the number of bath modes, $R_{i\alpha}$ ($p_{i\alpha}$) the position (momentum) of bath mode α for bath i, m the mass (assumed to be same for all bath modes without loss of generality), and $\omega_{i\alpha}$ the frequency of bath mode α. Finally, the coupling between the electronic system and the nuclear bath of harmonic oscillators is given by

$$H_{\mathrm{eb}} = \sum_{i=1}^{M} \sum_{\alpha=1}^{N} c_{i\alpha} R_{i\alpha} d_i^\dagger d_i \tag{8}$$

The couplings $c_{i\alpha}$ are given by the spectral density

$$J_i(\omega) = \frac{\pi}{2} \sum_{\alpha} \frac{{c_{i\alpha}}^2}{m\omega_{i\alpha}} \delta(\omega - \omega_{i\alpha}) \tag{9}$$

In practice, below we will assume that each bath corresponds to the same Drude spectral density $J_i(\omega) = J(\omega)$:

$$J(\omega) = 2V_{\mathrm{r}} \frac{\gamma\omega}{\omega^2 + \gamma^2} \tag{10}$$

where V_{r} is the reorganization energy and $1/\gamma$ is the bath response time. In practice, when necessary, this bath can be discretized numerically; see section 3.4.2 for details.

The total Hamiltonian, including the interaction of the molecular system with light, is given by

$$H = H_{\mathrm{mol}} - \boldsymbol{\mu} \cdot \mathbf{E}(t) \tag{11}$$

where H_{mol} is the Hamiltonian of the matter and $\mathbf{E}(t)$ is the electromagnetic field. $\boldsymbol{\mu}$ is the dipole moment operator

$$\boldsymbol{\mu} = \mu_+ + \mu_- \tag{12}$$

with

$$\mu_+ = \sum_{i=1}^{M} {\mu_i}^0 d_i^\dagger \tag{13}$$

$$\mu_- = \sum_{i=1}^{M} {\mu_i}^0 d_i \tag{14}$$

Note that we make the Condon approximation in the site and excitonic bases; i.e., μ_i^0 are numbers independent of the bath modes.

The parameters used in this work are the same as used in ref 44 and are listed in Table 1. These parameters represent a dimer system in the presence of an overdamped Brownian oscillator bath with an inhomogeneous broadening of 198 cm^{-1}. The parameters chosen are such that the system is in the inhomogeneous regime. When describing our augmented fewest switches surface hopping (AFSSH) approach in section 3.4, we will provide a general ansatz for arbitrary M; however, all results in section 4 will be presented only for the case M = 2, i.e., a pair of two level systems, so that

DOI: 10.1021/acs.jpcb.8b08674
J. Phys. Chem. B XXXX, XXX, XXX−XXX

Table 1. Parameters for the Model Hamiltonian[a]

parameter	value
ϵ_1	-250 cm^{-1} (relative to 10 000 cm^{-1})
ϵ_2	250 cm^{-1} (relative to 10 000 cm^{-1})
V_c	100 cm^{-1}
N	2000
V_r	94.4 cm^{-1}
γ	4.47 ps^{-1}
T	300 K
μ_1^0	1
μ_2^0	1

[a]These parameters are the same as in ref 44.

$$H_{\mathrm{el}} = \sum_{i=1}^{2} \epsilon_i d_i^\dagger d_i + V_c(d_1 d_2^\dagger + d_2 d_1^\dagger) \tag{15}$$

As far as notation is concerned, in this paper, we use i, j to denote orbitals in a site basis (as above). In section 3.3, the indices l, m, n, and p denote excitonic electronic orbitals [i.e., orbitals that arising from diagonalization of the electronic Hamiltonian at the minimum geometry of the bath]; in section 3.4, l, m, n, and p denote adiabatic electronic orbitals that can depend on nuclear (bath) position.

Finally, when dealing with spectroscopy, one often requires the ability to index the set of many-body electronic states. For instance, in the case of an *ab initio* calculation, one would like to compute true excited states (rather than just working with a Fock matrix and a set of orbitals). Now, for the Frenkel Hamiltonian above, it is easy to associate a singly excited many-body electronic state with a single orbital: each singly excited state exactly corresponds to one excited orbital. However, for the doubly excited many-body excited state, obviously one must specify two single orbitals for excitation. Although it might not seem natural, henceforward, we will let q denote a doubly excited state $|q\rangle$ in any basis. We emphasize that q does not index an orbital, but rather a pair of excited orbitals.

For clarity, as an example, consider a system with two spinless electrons and a pair of orbitals (on the left and right), i.e., the situation treated in section 4. Recall that the Fock space is four-dimensional: there is the ground state $|1\rangle = |00\rangle$, a singly excited state on the left $|2\rangle = |10\rangle$, a singly excited state on the right $|3\rangle = |01\rangle$, and a doubly excited state $|4\rangle = |11\rangle$. For this model problem, the set of single orbitals $\{i, j\}$ is isomorphic to the set of single excitations, $\{2, 3\}$. There is only a single doubly excited state $|q\rangle = |4\rangle$. See Figure 2. Henceforward, we will denote μ_{nq} as the dipole matrix element between a singly excited state $|n\rangle$ and a doubly excited state $|q\rangle$.

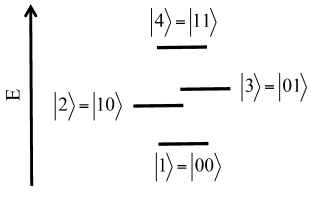


Figure 2. Pictorial representation of the energy level diagram. The state $|00\rangle$ is the ground state, $|10\rangle$ and $|01\rangle$ are singly excited states, and $|11\rangle$ is the doubly excited state.

3. THEORY

3.1. 2D Spectroscopy. We assume that the electromagnetic field applied is weak enough such that perturbation theory is applicable. In this weak interaction regime, the 2D spectra can be computed from the third order response, with the polarization $P(t)$ given by[46,47]

$$\mathbf{P}(\mathbf{t}) = \left(\frac{\mathrm{i}}{\hbar}\right)^3 \int_0^\infty \mathrm{d}t_3 \int_0^\infty \mathrm{d}t_2 \int_0^\infty \mathrm{d}t_1\, \mathbf{E}(t-t_3)\, \mathbf{E}(t-t_3-t_2) \times \mathbf{E}(t-t_3-t_2-t_1)\, R(t_3,t_2,t_1) \tag{16}$$

where R is the response function

$$R(t_3,t_2,t_1) = \langle[[[\mu(t_3+t_2+t_1), \mu(t_2+t_1)], \mu(t_1)], \mu(0)]\rho(0)\rangle \tag{17}$$

Here, $\rho(0)$ is the equilibrium system density matrix and $\mu(t)$ is the dipole moment operator in the interaction representation: $\mu(t) = \mathrm{e}^{\mathrm{i}H_{\mathrm{mol}}t}\mu\mathrm{e}^{-\mathrm{i}H_{\mathrm{mol}}t}$.

Note that $R(t)$ is a purely imaginary function;[48] in many textbooks (e.g., Mukamel[47]), one multiplies $R(t)$ by i, so that $R(t)$ is real. In any event, the observable third-order polarization $P(t)$ is clearly real and, for the case of δ-function pulses, $P(t) \propto \mathrm{i}R(t_3,t_2,t_1)$;[49] the 2D absorption spectrum is the 2D half Fourier transform of the signal $P(t)$, i.e.

$$\mathrm{Re}\, S(\omega_1,t_2,\omega_3) = \mathrm{Re} \int_0^\infty \mathrm{d}t_1 \int_0^\infty \mathrm{d}t_3\, \mathrm{e}^{\mathrm{i}\omega_1 t_1}\mathrm{e}^{\mathrm{i}\omega_3 t_3} R(t_3,t_2,t_1) \tag{18}$$

Thus, all that remains is to calculate the response function $R(t_3,t_2,t_1)$.

For the Hamiltonian of eqs 5−8, this response function can be written as the sum of rephasing and nonrephasing components

$$R(t_3,t_2,t_1) = R_{\mathrm{rp}}(t_3,t_2,t_1) + R_{\mathrm{nr}}(t_3,t_2,t_1) \tag{19}$$

As is standard, we will focus on those response terms that do not involve double excitations of the state at time $t_1 + t_2$. These terms are

$$R_{\mathrm{rp}}(t_3,t_2,t_1) = \phi_1(t_3,t_2,t_1) + \phi_2(t_3,t_2,t_1) - \phi_3(t_3,t_2,t_1) \tag{20}$$

$$R_{\mathrm{nr}}(t_3,t_2,t_1) = \phi_4(t_3,t_2,t_1) + \phi_5(t_3,t_2,t_1) - \phi_6(t_3,t_2,t_1) \tag{21}$$

The individual components $\phi_1 - \phi_6$ correspond to different Feynman pathways and are shown pictorially in Figure 3. Using the notation in eqs 13 and 14, we can write the explicit form of these terms as

$$\phi_1(t_3,t_2,t_1) = \langle \mu_-(t_3+t_2+t_1)\, \mu_+(t_1)\, \rho(0)\, \mu_-(0)\, \mu_+(t_1+t_2)\rangle \tag{22}$$

$$\phi_2(t_3,t_2,t_1) = \langle \mu_-(t_3+t_2+t_1)\, \mu_+(t_2+t_1)\, \rho(0)\, \mu_-(0)\, \mu_+(t_1)\rangle \tag{23}$$

$$\phi_3(t_3,t_2,t_1) = \langle \mu_-(t_3+t_2+t_1)\, \mu_+(t_2+t_1)\, \mu_+(t_1)\, \rho(0)\, \mu_-(0)\rangle \tag{24}$$

$$\phi_4(t_3,t_2,t_1) = \langle \mu_-(t_3+t_2+t_1)\, \mu_+(0)\, \rho(0)\, \mu_-(t_1)\, \mu_+(t_1+t_2)\rangle \tag{25}$$

$$\phi_5(t_3,t_2,t_1) = \langle \mu_-(t_3+t_2+t_1)\, \mu_+(t_1+t_2)\, \mu_-(t_1)\, \mu_+(0)\, \rho(0)\rangle \tag{26}$$

DOI: 10.1021/acs.jpcb.8b08674
J. Phys. Chem. B XXXX, XXX, XXX−XXX

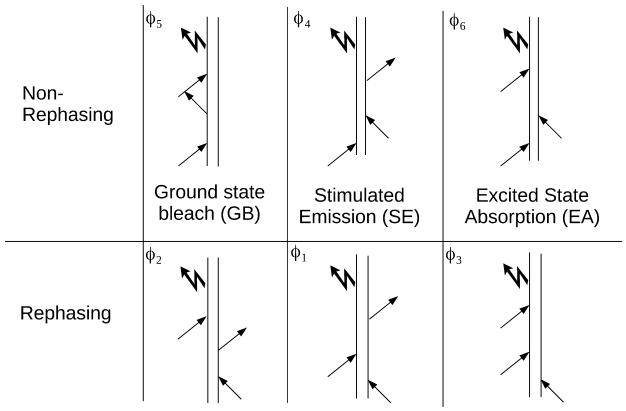


Figure 3. Feynman diagrams for the different pathways listed in eqs 22−27.

$$\phi_6(t_3,t_2,t_1) = \langle \mu_-(t_3+t_2+t_1)\, \mu_+(t_1+t_2)\, \mu_+(0)\, \rho(0)\, \mu_-(t_1)\rangle \tag{27}$$

Again following convention, in eqs 20−27, we have not written down the relevant terms which would correspond to emission from the bra; mathematically all such terms with $\mu_+(t_3+t_2+t_1)$ instead of $\mu_-(t_3+t_2+t_1)$ correspond to the complex conjugates of eqs 22−27 and we ought to write, e.g.,

$$R_{rp}(t_3,t_2,t_1) = 2i\mathrm{Im}(\phi_1(t_3,t_2,t_1)) + 2i\mathrm{Im}(\phi_2(t_3,t_2,t_1)) - 2i\mathrm{Im}(\phi_3(t_3,t_2,t_1)) \tag{28}$$

To simplify eqs 18−21, one can make the rotating wave approximation (which is equivalent to phase-matching in spectroscopy), so that we can write

$$\mu\cos(\omega t) = \mu_+ e^{i\omega t} + \mu_- e^{-i\omega t} \tag{29}$$

Or, in other words, we ignore all terms of the form $\mu_+ e^{-i\omega t}$ or $\mu_- e^{+i\omega t}$. And with this approximation, if we shift the nonrephasing signal from $+\omega_1$ to $-\omega_1$, our final expression becomes

$$S(\omega_1,t_2,\omega_3) = S_{rp}(\omega_1,t_2,\omega_3) + S_{nr}(\omega_1,t_2,\omega_3) \tag{30}$$

where

$$S_{rp}(\omega_1,t_2,\omega_3) = \int_0^\infty dt_1 \int_0^\infty dt_3\, [e^{i(-\omega_1 t_1+\omega_3 t_3)}\, R_{rp}(t_3,t_2,t_1)] \tag{31}$$

$$S_{nr}(\omega_1,t_2,\omega_3) = \int_0^\infty dt_1 \int_0^\infty dt_3\, [e^{i(\omega_1 t_1+\omega_3 t_3)}\, R_{nr}(t_3,t_2,t_1)] \tag{32}$$

The signals S_{rp} and S_{nr} include both real and imaginary components. In practice, we will plot and analyze the real parts of these spectra below. We will now describe two standard approaches for computing this 2D spectra, an HEOM and cumulant approach, against which we will compare our results below.

3.2. HEOM Approach. For the model problem in eqs 5−8 with a Debye spectral density, Chen et al.[30,31] have shown that one can construct exact 1D and 2D spectra using a hierarchical equation of motion (HEOM) approach.[50,51] This methodology propagates the density matrix numerically, requiring a growing number of auxiliary density matrices to converge the dynamics for longer and longer periods of time. In this work we follow closely the approach in ref 51. Simulations are evolved for $t_1 = t_3 = 250$ fs with a time step of 1 fs. Only the first matsubara frequency is kept, and converged results are obtained with a hierarchy $L = 15$. The integrals in eqs 31 and 32 are computed numerically with frequencies ω_1 and ω_3 discretized using 100 points from −800 to 800 cm^{-1}.

3.3. Cumulant Expansion. Apart from an exact HEOM calculation, an approximate alternative is to compute 2D spectra through a cumulant expansion, as was discussed in the Introduction. For this approach to be operational (without any modification), we must make an additional assumption—namely, all nonadiabatic dynamics must be ignored (over all times). In practice, this means that we will work in the excitonic basis (i.e., the eigenfunction the basis of H_{el} in eq 6), where analytical results can be computed, and assume that the baths couple to the excitonic states independently; we will ignore population relaxation from one excitonic state to another as induced through nuclear motion (which in turn induces diabatic coupling). As one might expect, this approach leads to good results for $t_2 = 0$, but the quality of these results deteriorates for long t_2 times (because we ignore all nonadiabatic dynamics).

To derive the standard form for the 2D line shape, one follows the same steps as in deriving the expression for the 1D spectra in eq 3. We compute the average frequency−frequency time correlation functions, and the Kubo-line shape function $g(t)$ is defined by

$$g_{mn}(t) = \int_0^t d\tau' \int_0^{\tau'} d\tau''\, \langle \delta\tilde{\Omega}_m(\tau'')\, \delta\tilde{\Omega}_n(0)\rangle \tag{33}$$

Here, $\tilde{\Omega}_m$ is the energy of exciton m relative to the ground state, $\tilde{\Omega}_m = H_m - H_g$.

With the definition of $g(t)$ above, we can simplify eqs 22−27 for the case of two molecules to obtain the signals in eqs 31 and 32. All detailed equations as required by a cumulant expansion for this calculation are shown in Appendix A. Note that, in practice, in order to simplify our equations, we will take a partially classical limit and ignore the imaginary part of $g(t)$.

At this point, all that remains is to calculate $g(t)$. For the special case considered by Kubo, one imagines the following form for the correlation function,

$$\langle \delta\tilde{\Omega}_m(t)\, \delta\tilde{\Omega}_n(0)\rangle = \Delta_{mn}{}^2 e^{-t/\tau_c} \tag{34}$$

so that one can calculate (from eq 33)

$$g_{mn}(t) = \Delta_{mn}{}^2 \tau_c{}^2 \left[e^{-t/\tau_c} + \frac{t}{\tau_c} - 1 \right] \tag{35}$$

Here, Δ_{mn} quantifies the correlations of the energy fluctuations for different excitonic states and τ_c is the relaxation time for the bath. Below, we will assume that the relaxation time scale τ_c is the same for all baths.

Now, in general, the parameters Δ_{mn} and τ_c must be extracted from a molecular dynamics simulation (after fitting). While these correlation functions should be calculated quantum mechanically in principle (see Appendix A), for our purposes in this paper, we will simply compute real, classical correlation functions with motion along the ground state. Furthermore, using the Drude spectral density in eq 10, these quantities can be calculated analytically within a reasonable approximation. To see this, note that, in the site basis, the frequency−frequency autocorrelation function is given exactly by

DOI: 10.1021/acs.jpcb.8b08674
J. Phys. Chem. B XXXX, XXX, XXX−XXX

$$\langle \delta\Omega_i(t)\, \delta\Omega_j(0)\rangle = \Delta^2 e^{-t/\tau_c}\delta_{ij} \tag{36}$$

where $\Delta = \sqrt{2k_B T V_r}$ and $\tau_c = 1/\gamma$; see Appendix B for a derivation. In a similar spirit, if we transform to the excitonic basis, since the site to exciton transformation U is time independent and all dynamics are assumed to be on the ground state, we find

$$\langle \delta\tilde{\Omega}_m(t)\, \delta\tilde{\Omega}_n(0)\rangle = \sum_{ij} U_{im}U_{jm}U_{in}U_{jn}\langle \delta\Omega_i(t)\, \delta\Omega_j(0)\rangle \tag{37}$$

$$= \sum_i U_{im}{}^2 U_{in}{}^2 \Delta^2 e^{-t/\tau_c} \tag{38}$$

so that we have now recovered eq 34 with

$$\Delta_{mn} = \Delta \sum_i U_{im}{}^2 U_{in}{}^2 \tag{39}$$

For the parameters listed in Table 1, the excitonic energies are $\tilde{\epsilon}_1 = -269.2$ cm^{-1} and $\tilde{\epsilon}_2 = 269.2$ cm^{-1} and the dipole moments are $\tilde{\mu}_1 = -0.79$ and $\tilde{\mu}_2 = 1.17$. Using eq 39, we obtain $\Delta_{11} = \Delta_{22} = 184.7$ cm^{-1}, $\Delta_{12} = \Delta_{21} = 13.7$ cm^{-1} and $\tau_c = 224$ fs. Numerical integrals of eqs 94−99 are computed with cutting the t_1 and t_3 integrals at 200 fs with a step of 2 fs. The frequencies ω_1 and ω_3 range from −800 to +800 cm^{-1} equally spaced over a grid of 100 points.

3.4. Surface Hopping Approach. HEOM methods and cumulant expansions are powerful approaches for computing spectra. However, these approaches also have limitations. On the one hand, HEOM assumes a harmonic bath with bilinear couplings and can be expensive. On the other hand, a cumulant expansion ignores all nonadiabatic dynamics. The aim of the present work is to provide an alternative approach that can overcome these limitations at minimal cost (and ideally with minimal loss of accuracy).

Our ansatz is to build upon methods developed recently in the Jansen group[44] for computing spectra semiclassically, and thus with minimal cost and no harmonic restrictions. In ref 44, Jansen et al. developed semiclassical sampling tools for reconstructing the three-time response function in eq 17. The general framework is to propagate nuclear dynamics along the quantum ground state during coherence times t_1 and t_3, and then to run surface hopping, or Ehrenfest dynamics, during waiting time t_2. During all three time periods, t_1, t_2, and t_3, one continuously evolves the electronic wave function. In the end, from this data, ref 44 demonstrates that one can extract reasonably good spectra. And yet, for our purposes (which are to use *ab initio* electronic structure theory), these methods may still be too expensive for application to large systems of interest.

To simplify further the Jansen approach, we will now attempt to decouple (when possible) the t_2 waiting time dynamics from the t_1 and t_3 coherent dynamics. To be precise, for the t_1 and t_3 dynamics, we wish to invoke an inhomogeneous ansatz for the line shape, whereby we can extract a spectrum by merely sampling an energy gap (and not running dynamics). Through such a huge simplification, we can dramatically enhance the computational efficiency of the method, and for some inhomogeneous cases, we will show that we can still obtain accurate results. To understand the details of our proposed approach, let us first discuss the line shape of $t_2 = 0$ spectra (before turning to the full spectral expressions for $t_2 \geq 0$.).

3.4.1. Line Shape of $t_2 = 0$ Spectra. Our overall goal is to compute 2D spectra while running dynamics only for the t_2 waiting time. Thus, for spectra taken with zero waiting time ($t_2 = 0$), we require a simple, dynamics-free expression for the 2D spectral line shape. For this purpose, we are guided by Kubo's well-known transformation whereby, in the inhomogeneous limit, a two-state linear absorption spectrum ($I(\omega)$ in eq 1) takes the form of a histogram in energy space ($I(\omega)$ in eq 4). Thus, for a linear absorption spectrum, one needs only to sample the excitation energies and, in the inhomogeneous limit, it is standard to assume the absorption spectrum has a Gaussian form:

$$I(\omega) \propto \mu_{12}{}^2 \exp\left[-\frac{(\omega - \omega_{21})^2}{2\sigma^2}\right] \tag{40}$$

Here, $\omega_{21} = V_2 - V_1$, where V_i are the eigenfunctions of the Hamiltonian $H_{el} + H_{eb}$.

To illustrate the validity of the inhomogeneous ansatz, for the Hamiltonian in section 2, Figure 4 compares the exact linear absorption spectrum as computed using the HEOM method versus the inhomogeneous spectrum as computed with a simple binning approach. The HEOM results are computed with an evolution of 2.5 ps, and frequency discretized from −1000 to +1000 cm^{-1} with 100 grid points. The binning results are computed by averaging over 100 000 trajectories with 101 grid points, again with frequency discretized from −1000 to +1000 cm^{-1}. Note that binning results have no explicit dynamics; this method computes the spectra by simply binning the adiabatic energy differences starting with a thermal distribution on the ground electronic state. The excellent agreement in Figure 4 shows the validity of binning for the regimes analyzed in this work.

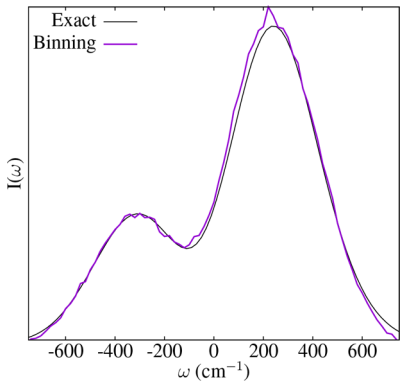


Figure 4. Normalized absorption spectra computed using HEOM and a simple binning approach. All energies on the x-axis are relative to 10 000 cm^{-1}, the unshifted vertical energy gap. Note that no dynamics is performed for the binning approach. See text for numerical details, e.g., the number of bins, etc.

With this analogy in mind, in the inhomogeneous limit, we would like to consider a 2D spectrum (with multiple electronic states) to be the correlation function between the energy of a system at time t_1 (ω_1) and the energy of the system at time $t_1 + t_2$ (ω_3), $I(\omega_1,t_2,\omega_3) \sim \langle \delta(\omega_1 - \omega(t_1))\, \delta(\omega_3 - \omega(t_1+t_2))\rangle = \langle \delta(\omega_1 - \omega(0))\, \delta(\omega_3 - \omega(t_2))\rangle$, where the ensemble averaging must implicitly include the bath-dependent adiabatic transition dipole moments.[52] But, of course, this simplification does not agree with experiment. For example, see the cartoon in Figure

DOI: 10.1021/acs.jpcb.8b08674
J. Phys. Chem. B XXXX, XXX, XXX−XXX

5. Even with $t_2 = 0$, the 2D spectrum shows broadening along the diagonal peak and, in the rotated coordinates

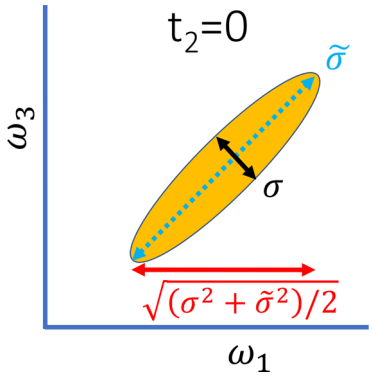


Figure 5. Cartoon of a 2D spectrum at $t_2 = 0$. Note that, even with zero waiting time, there is a width to every diagonal peak, σ, reflecting the homogeneous broadening of the line shape.

$$f_1 \equiv \frac{1}{\sqrt{2}}(\omega_1 - \omega_3) \tag{41}$$

and

$$f_3 \equiv \frac{1}{\sqrt{2}}(\omega_1 + \omega_3) \tag{42}$$

the signal might best be considered to be of the form

$$I(f_1,0,f_3) \propto \sum_K \exp\left[-\frac{(f_3 - \lambda_K)^2}{2\tilde{\sigma}^2}\right]\exp\left[-\frac{f_1^2}{2\sigma^2}\right] \tag{43}$$

In standard coordinates, this can be expressed as

$$I(\omega_1,0,\omega_3) \propto \sum_K \exp\left[-\frac{(\omega_1 + \omega_3 - \sqrt{2}\lambda_K)^2}{4\tilde{\sigma}^2}\right] \times \exp\left[-\frac{(\omega_1 - \omega_3)^2}{4\sigma^2}\right] \tag{44}$$

where $\lambda_K/\sqrt{2}$ is the transition frequency for the Kth excited state.

Here, we will call σ the off-diagonal broadening, while $\tilde{\sigma}$ reflects the fluctuations along the diagonal; it is straightforward to show that the overall fluctuations of the instantaneous energies $\delta\omega = \omega - \langle\omega\rangle$ have standard deviation $(\sigma^2 + \tilde{\sigma}^2)/2$. While we may safely assume that the spread in frequencies ($\tilde{\sigma}$) arises from the inhomogeneous equilibrium ensemble and t_2 dynamics, the off-diagonal broadening (σ) arises because of homogeneous effects. For a rigorous theory of this broadening, we would need to run dynamics during t_1 and t_3, and then Fourier transform (as in HEOM). Thus, if we are to avoid running such dynamics, we will require a simple means to evaluate this broadening parameter. Note that we will assume that the rate of nonadiabatic population transfer during the t_1 and t_3 coherence times is slower than the rate of dephasing, such that nonadiabatic population transfer can be ignored when computing the final signal.

To make progress here, we focus on exactly one diagonal peak in the ground state bleach spectrum centered at $(\omega_1, \omega_3) = (\lambda/\sqrt{2}, \lambda/\sqrt{2})$. We will estimate σ as the off-diagonal broadening for such a ground state bleach spectrum (arising from ϕ_2 and ϕ_5 in eqs 23 and 26), ignoring the contributions from all but one excited state (in this case, chosen as an excitonic state). Referring to the expressions for the cumulant expansion in Appendix A, and specifically eq 95 (but with only one excited state), we write the real part of the rephasing ground state bleach signal (within the cumulant expansion approach) as

$$\mathrm{Re}\ S_2(\omega_1,0,\omega_3) = \mathrm{Re}\int_0^\infty dt_1 \int_0^\infty dt_3\ e^{-i\delta\omega_1 t_1} e^{i\delta\omega_3 t_3} e^{-2g(t_1)-2g(t_3)+g(t_1+t_3)} \tag{45}$$

Similarly, in analogy with eq 98 (but with only one excited state), the real part of the nonrephasing ground state bleach signal is given by

$$\mathrm{Re}\ S_5(\omega_1,0,\omega_3) = \mathrm{Re}\int_0^\infty dt_1 \int_0^\infty dt_3\ e^{i\delta\omega_1 t_1} e^{i\delta\omega_3 t_3} e^{-g(t_1+t_3)} \tag{46}$$

In eqs 45 and 46, we have defined $\delta\omega_1 = \omega_1 - \lambda/\sqrt{2}$ and $\delta\omega_3 = \omega_3 - \lambda/\sqrt{2}$, and $g(t)$ is defined in eq 35.

To compute the off-diagonal broadening, we rotate our coordinates with a change of variables, $f_1 = \frac{1}{\sqrt{2}}(\delta\omega_1 - \delta\omega_3)$, $f_3 = \frac{1}{\sqrt{2}}(\delta\omega_1 + \delta\omega_3)$, $t = \frac{1}{\sqrt{2}}(t_1 + t_3)$ and $t' = \frac{1}{\sqrt{2}}(t_1 - t_3)$. With this transformation, we recover

$$\mathrm{Re}\ S_2(f_1,0,f_3) = \mathrm{Re}\int_0^\infty dt \int_{-t}^{t} dt'\ e^{-if_1 t} e^{if_3 t'} \times e^{-2g((t+t')/\sqrt{2})-2g((t-t')/\sqrt{2})+g(\sqrt{2}t)} \tag{47}$$

$$\mathrm{Re}\ S_5(f_1,0,f_3) = \mathrm{Re}\int_0^\infty dt \int_{-t}^{t} dt'\ e^{if_1 t'} e^{if_3 t} e^{-g(\sqrt{2}t)} \tag{48}$$

Now, to estimate σ, we compute the total signal

$$\mathrm{Re}\ S(f_1,0,f_3) = \mathrm{Re}\ S_2(f_1,0,f_3) + \mathrm{Re}\ S_5(f_1,0,f_3) \tag{49}$$

at $f_3 = 0$, and fit the resulting one-dimensional signal $S(f_1,0,0)$ to a Gaussian. The width of the Gaussian is taken to be σ.

We emphasize again that, in eqs 47 and 48 we have considered only one two level system coupled to a bath. For the case of multiple levels or chromophores coupled to baths (see below), we will make one more critical assumption, i.e., that σ is the same for all peaks. In practice, the different peaks may well have different homogeneous broadenings, but for convenience, we will ignore that possibility. When invoking eqs 47 and 48, we are also assuming that the f_1-moment of $S(f_1,0,f_3)$ is fairly independent of the value of f_3, and so we may safely evaluate the moment σ by considering only $S(f_1,0,0)$. Altogether, these assumptions will make it far easier to construct an efficient, simplified surface hopping theory of 2D spectroscopy. As a practical matter, as t_2 grows, we find that the effect of the broadening parameter is usually washed away as inhomogeneous broadening takes over. Nevertheless, in order to compute an accurate spectra for small t_2, it is crucial to ascertain an accurate estimate of σ.

For the parameters listed in Table 1, we numerically evaluated eqs 47 and 48 and the result is plotted in Figure 6. Fitting this result to a Gaussian gives $\sigma = 80\ \mathrm{cm}^{-1}$; note that the agreement is fairly good. The integrals are numerically computed using a maximum time for t of 1 ps with a time step of 1 fs, and discretized frequency f_1 from −500 to +500 cm^{-1} using an equally spaced grid of 1000 points. In performing this

DOI: 10.1021/acs.jpcb.8b08674
J. Phys. Chem. B XXXX, XXX, XXX−XXX

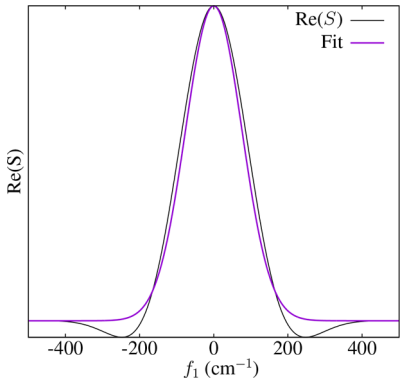


Figure 6. (Black) off-diagonal signal Re $S(f_1,0,0)$ as computed using eq 49 using the parameters in Table 1. (Red) Gaussian fit of the form $g(f_1) \equiv g_0 e^{-f_1^2/2\sigma^2}$. After performing a fit, we find a broadening parameter σ = 80 cm^{-1}.

analysis, we have evaluated the 2D ground state bleach spectrum around the peak $\omega_1 = \omega_3$ = 10000−267 cm^{-1}; however, for the model Hamiltonian in eqs 5−8, the same result would be found for both diagonal peaks (10000 ± 267 cm^{-1}). To verify that σ is approximately independent of the value of f_3 used in the evaluation of eqs 47 and 48, we also computed the integrals for f_3 = 100 cm^{-1} and f_3 = 400 cm^{-1}. These different values of f_3 had negligible effect on the value of σ.

3.4.2. Computing $t_2 \geq 0$ Spectra. We will now give concrete expressions for calculating $t_2 \geq 0$ 2D spectra, separately treating the cases of ground state bleach, stimulated emission, and excited state absorption.

Our basic ansatz is that we will run dynamics, sampling trajectories with Gaussians of width σ. In particular, for a trajectory at position $\vec{R}$ with energy gap ω_{n1} between adiabatic excited state n and the ground state 1 at time t, we denote a normalized Gaussian in frequency space:

$$b_{n1}(\omega,t) = \frac{1}{\sqrt{2\pi\sigma^2}} \exp\left[-\frac{(\omega - \omega_{n1}(\vec{R}(t)))^2}{2\sigma^2}\right] \tag{50}$$

Recall that we are indexing adiabatic electronic orbitals with l, m, n, p, and 1 is the ground state. When calculating the signal $\phi_1 - \phi_6$ in eqs 22−27, we will sometimes require surface hopping (SH) dynamics and other times we will require adiabatic dynamics, either along the ground state (GS) or along the average of two state, e.g., n and m, so that $V_{\text{av}}^{n+m} = \frac{1}{2}(V_n + V_m)$.

As far as initial conditions are concerned, we sample all nuclear geometries from a Boltzmann distribution equilibrated to the electronic ground state. For computing stimulated emission and excited state absorption components, the electronic density matrix is initialized to correspond to an excitation from a photon field; i.e., we set the quantum coefficients to be

$$c_n = \frac{\mu_{1n}}{\sqrt{\sum_p |\mu_{1p}|^2}} \tag{51}$$

The corresponding density matrix is

$$\rho_{nm} = c_n c_m^* = \frac{\mu_{1n}\mu_{1m}^*}{\sum_p |\mu_{1p}|^2} \tag{52}$$

Henceforward, when we write a bracket $\langle X \rangle$, this implies averaging the operator X over trajectories. For all surface hopping trajectories, we will follow the details in ref 53 with a 2 fs time step. The GSB, SE, and ESA components of the 2D spectrum are each calculated by averaging over 10 000 trajectories. For the stimulated emission/excited state absorption trajectories, the probability of initializing a population on excited state n is proportional to $|\mu_{1n}|^2$ and the probability of initializing a coherence between excited states n and m is proportional to $2|\mu_{1n}\mu_{1m}|$. Regarding eq 10, each bath is discretized with 2000 equally spaced frequencies with the maximum frequency being 794 cm^{-1}. The mass of each bath mode is 5 amu. The frequencies ω_1 and ω_3 are discretized using 101 points between −800 and +800 cm^{-1}.

Ground State Bleach. Because the ground state bleach signal does not involve any excited state dynamics during the t_2 time, this pathway represents the simplest case. Within the framework set up above, our expression for the rephasing and nonrephasing signals are equal and given by

$$\begin{aligned}\phi_2(\omega_1,t_2,\omega_3) &= \phi_5(\omega_1,t_2,\omega_3) \\ &= \sum_{nm} \langle |\mu_{1m}(0)|^2 |\mu_{1n}(t_2)|^2 B_{mn}^{\text{GS}}(\omega_1,0;\omega_3,t_2)\rangle\end{aligned} \tag{53}$$

The ground state bleach broadening is chosen to be

$$B_{mn}^{\text{GS}}(\omega_1,0;\omega_3,t_2) = b_{1m}(\omega_1,0)\, b_{1n}(\omega_3,t_2) \tag{54}$$

and $\mu_{1n}(t_2)$ is the dipole moment matrix element evaluated between the ground state and adiabatic state n at time t_2. All dynamics are initially sampled from the ground state equilibrium distribution and propagated along the ground state as well. For the specific model problem in section 2 with only a pair of molecules, there were only two bright states; therefore, $\sum_{nm}$ in eq 7 are only over two states, n, m = {2, 3}.

Stimulated Emission. For the case of stimulated emission, t_2 dynamics occur on the singly excited state manifold, and there is transfer of intensity from diagonal to off-diagonal peaks in the 2D spectra as a function of t_2. Here, a natural ansatz for the nonrephasing signal ϕ_1 would be

$$\begin{aligned}&\phi_1(\omega_1,t_2,\omega_3) \\ &= \left\langle \sum_{l,m,n,p} \mu_{1l}(0)\, \mu_{m1}(0)\, \mu_{1n}(t_2)\, \mu_{p1}(t_2)\, \rho_{lm}^{np}(t_2)\, B(\omega_1,0;\omega_3,t_2) \right\rangle\end{aligned} \tag{55}$$

Besides the weighting function $B(\omega_1,0;\omega_3,t_2)$, the key dynamical quantity to compute is $\rho_{lm}^{np}(t_2)$: the (n,p)th density matrix element at time t_2 given that the density matrix was initialized as (l, m) at t_2 = 0. Obviously, $\rho_{lm}^{np}(t_2=0) = \delta_{l,n}\delta_{m,p}$. More generally, however, the calculation of $\rho_{lm}^{np}(t_2)$ can be very difficult because it requires effectively two different classes of calculations with different initialization criteria:

- On the one hand, when $l = m$, the system starts in a population, and so initialization of surface hopping trajectories is very straightforward.
- On the other hand, when $l \neq m$, the system starts in a coherence, and so initialization of surface hopping trajectories is far less natural, as shown by the

DOI: 10.1021/acs.jpcb.8b08674
J. Phys. Chem. B XXXX, XXX, XXX−XXX

underperformance of surface hopping for recovering absorption spectroscopy.[22,54,55] For this reason, for an initial coherence between adiabats n and m, we will simply follow the quantum-classical Liouville equation and propagate nuclei on the potential,

$$V_{av}^{n+m} = \frac{1}{2}(V_n + V_m) \tag{56}$$

Given the above mismatch in techniques depending on the initial conditions, and given our desire for simplicity, we will make a big "secular" simplification. We will assume henceforward that

- If the system begins in a population at time $t_2 = 0$, we will measure only a population at time t_2. Thus, we measure $\rho_{mm}^{nn}(t)$ by initializing with active surface m and measuring the probability to be on active surface n at time t.
- If we begin in a $n - m$ coherence at time $t_2 = 0$, we can measure only a $n - m$ coherence at time t_2. Mathematically, we calculate $\rho_{nm}^{nm}(t)$ as $\rho_{nm}^{nm}(t) = \frac{\rho_{nm}(t)}{\rho_{nm}(0)}$, where all dynamics is along the surface $(V_n + V_m)/2$. This approximation is actually stronger than the previous assumption, because we do not allow for a change in coherence at all, only for a dephasing of the coherence. This ansatz is reasonable because, as a practical matter, we note that the effect of trajectories starting out as coherences tend to vanish by phase cancellation very quickly, and their effect disappears for most t_2 times.

Altogether, these approximations allow us to propagate populations and coherences entirely separately, leading to enormous computational savings. This ansatz was effectively suggested by the Reichmann group recently,[45] albeit in a more comprehensive context, where the authors found that, while propagating standard surface hopping trajectories for sampling populations, one could also spawn auxiliary trajectories to greatly improve predicted coherences following excitations.

Mathematically, we summarize our ansatz for ϕ_1 as follows:

$$\begin{aligned}\phi_1(\omega_1,t_2,\omega_3) &= \left\langle \sum_{m,n} |\mu_{1m}(0)|^2 |\mu_{1n}(t_2)|^2 \rho_{mm}^{nn}(t_2)\, B_{mn}^{\mathrm{SH}}(\omega_1,0;\omega_3,t_2) \right\rangle \\ &\quad + \left\langle \sum_{l<m} \mu_{1m}(0)\, \mu_{l1}(0)\, \mu_{1l}(t_2)\, \mu_{ml}(t_2)\, \rho_{lm}^{lm}(t_2)\, B_{lm}^{\mathrm{av}}(\omega_1,0;\omega_3,t_2) \right\rangle \end{aligned} \tag{57}$$

As far as the broadening functions are concerned, based on the Feynman diagrams of Figure 3, we make the following ansatz:

$$B^{\mathrm{SH}}(\omega_1,0;\omega_3,t_2) = b_{1m}(\omega_1,0)\, b_{1n}(\omega_3,t_2) \tag{58}$$

$$\begin{aligned}B_{lm}^{\mathrm{av}}(\omega_1,0;\omega_3,t_2) &= b_{1l}(\omega_1,0)\, b_{1l}(\omega_3,t_2) + b_{1m}(\omega_1,0)\, b_{1m}(\omega_3,t_2)\end{aligned} \tag{59}$$

All SH dynamics are initialized on active surface m, and all average (av) trajectories are propagated on surface $(V_l + V_m)/2$ in eq 57. As stated above, in all cases, the nuclear positions and momenta are sampled initially from the electronic ground state equilibrium distribution. Lastly, we estimate that the rephasing signal ϕ_4 should be the same as the nonrephasing signal ϕ_1, except that we include a slightly different broadening parameter (for the coherences as evolved on the average surface):

$$\begin{aligned}B_{lm}^{\mathrm{av}}(\omega_1,0;\omega_3,t_2) &= b_{1l}(\omega_1,0)\, b_{1m}(\omega_3,t_2) + b_{1m}(\omega_1,0)\, b_{1l}(\omega_3,t_2)\end{aligned} \tag{60}$$

Excited State Absorption. Finally, for the case of excited state absorption, all of the relevant mathematics is very analogous to the case of stimulated emission. The only essential difference is that the final state is not the ground state (but rather an excited state); in other words, for the Hamiltonian in section 2, the third pulse of light must promote the system to a doubly excited state. As discussed in section 2, this new situation leads to a slight notational complication, because now one cannot easily associate every excited electronic state with a single orbital. Nevertheless, once we label doubly excited states with an index q, we can easily construct excited state absorptive signals by analogy with stimulated emission. The relevant nonrephasing signal is

$$\begin{aligned}\phi_3(\omega_1,t_2,\omega_3) &= \left\langle \sum_{m,n,q} |\mu_{mm}(0)|^2 |\mu_{qn}(t_2)|^2 \rho_{mm}^{nn}(t_2)\, B_{nm}^{\mathrm{SH}}(\omega_1,0;\omega_3,t_2) \right\rangle \\ &\quad + \left\langle \sum_{q,l<m} \mu_{1m}(0)\, \mu_{l1}(0)\, \mu_{mq}(t_2)\, \mu_{ql}(t_2)\, \rho_{lm}^{lm}(t_2)\, B_{lm}^{\mathrm{av}}(\omega_1,0;\omega_3,t_2) \right\rangle \end{aligned} \tag{61}$$

The relevant broadening parameters are

$$B^{\mathrm{SH}}(\omega_1,0;\omega_3,t_2) = b_{1m}(\omega_1,0)\, b_{nq}(\omega_3,t_2) \tag{62}$$

$$\begin{aligned}B_{lm}^{av}(\omega_1,0;\omega_3,t_2) &= b_{1l}(\omega_1,0)\, b_{lq}(\omega_3,t_2) + b_{1m}(\omega_1,0)\, b_{mq}(\omega_3,t_2)\end{aligned} \tag{63}$$

As before, all SH dynamics are initialized on active surface m, and all average trajectories are propagated on surface $(V_l + V_m)/2$ in eq 61. As stated above, in all cases, the nuclear positions and momenta are sampled initially from the electronic ground state equilibrium distribution. For the rephasing signal ϕ_6, the expression is nearly unchanged, but the most natural broadening function (for the coherences as evolved on the average surface) is:

$$\begin{aligned}B_{lm}^{av}(\omega_1,0;\omega_3,t_2) &= b_{1l}(\omega_1,0)\, b_{mq}(\omega_3,t_2) + b_{1l}(\omega_1,0)\, b_{mq}(\omega_3,t_2)\end{aligned} \tag{64}$$

3.5. Algorithm. We now give a step-by-step outline for our heuristic algorithm for 2D optical spectra, as applicable to any condensed phase system (not just a Frenkel Hamiltonian):

- Compute the energy−energy autocorrelation function (eq 33), in either the excitonic or the adiabatic basis as would be necessary for an absorption calculation. This can be computed using simple ground state molecular dynamics and focusing on a single diagonal peak (e.g., the first bright excited state). Thereafter, one computes the broadening σ as the width of the Gaussian that best fits the function given in eq 49, using the $g(t)$ obtained from analyzing the energy−energy autocorrelation function. Our results above indicate that the calculated

DOI: 10.1021/acs.jpcb.8b08674
J. Phys. Chem. B XXXX, XXX, XXX−XXX

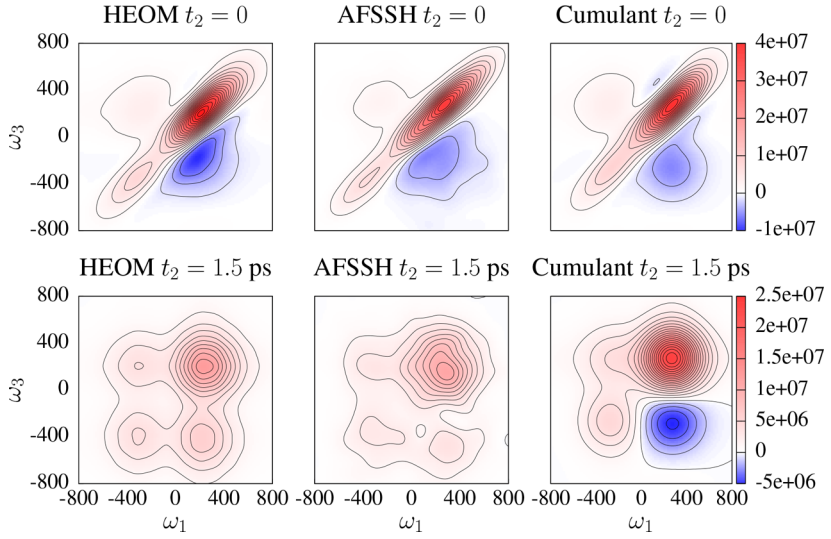


Figure 7. Comparison of the spectra computed using HEOM, AFSSH, and the cumulant expansion approach at t_2 = 0 ps and t_2 = 1.5 ps. Note that while the cumulant approach is accurate only for t_2 = 0, AFSSH is accurate for both long and short times.

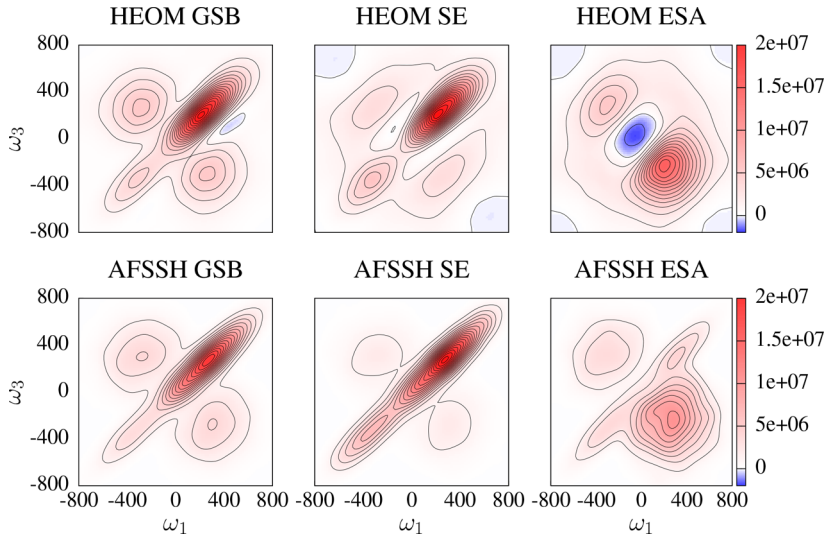


Figure 8. Comparison of the GSB, SE, and ESA components of the AFSSH and the HEOM spectra at t_2 = 0. The sum of the rephasing and nonrephasing signal is reported for each component. Note that AFSSH performs reasonably well, except for the negative feature in the electronic absorption signal (as predicted by HEOM but not by AFSSH). Note that the ESA component is subtracted from the GSB and SE components when the total signal is computed, giving negative features in Figure 7.

value of σ can be insensitive to the choice of f_3; furthermore, our hope is that, in many cases, one can safely perform this analysis without worrying too much about which peak we expand around.[56]

- Initialize the position and momentum of the bath modes for the Boltzmann distribution for the electronic ground state.
- Compute the ground state bleach components ϕ_2 and ϕ_5 using eq 53. For these equations, all trajectories are evolved only on the ground state for time t_2.
- Initialize the electronic density matrix as in eq 52, and compute stimulated emission and excited state absorption signals using eqs 57 and 61. Population dynamics are evolved using surface hopping, and coherence dynamics are evolved on an average potential energy surface (eq 56). Transitions between coherences and populations are neglected.

4. RESULTS

For the parameters in Table 1, in Figure 7, we plot the 2D spectra computed according to HEOM, surface hopping, and cumulant expansion, for t_2 = 0 and t_2 = 1.5 ps. From this figure, several features become clear. First, the AFSSH results are in excellent agreement with the exact results for both time values. Obviously, our approach was designed in part to replicate the t_2 = 0 spectra, and hence it should not be a big surprise that our results match almost exactly for t_2 = 0. Nevertheless, the key point is that the AFSSH method captures all of the features of the exact spectra at t_2 = 1.5 ps accurately. In particular, AFSSH captures the transfer of diagonal intensity to off-diagonal intensity, as well as the correct homogeneous broadening. As described in the Introduction, these are the two main features we wanted to recover accurately for comparison with experiment.

DOI: 10.1021/acs.jpcb.8b08674
J. Phys. Chem. B XXXX, XXX, XXX−XXX

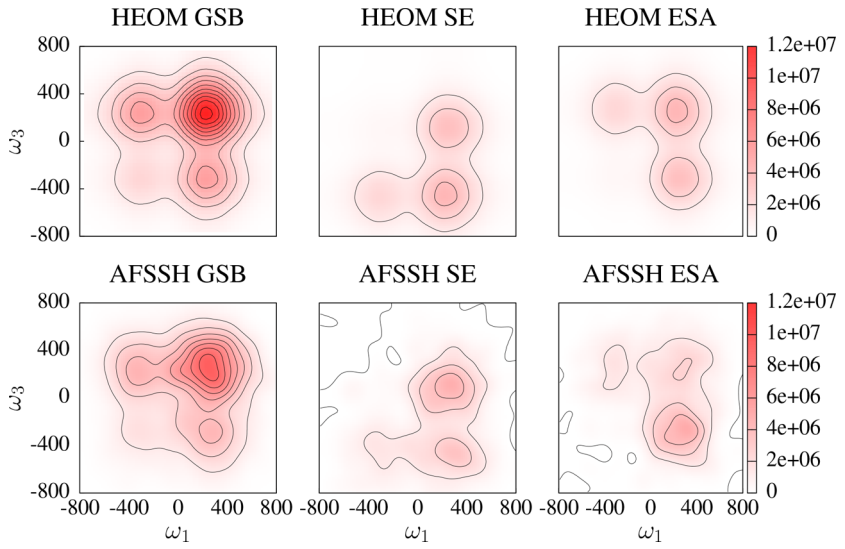


Figure 9. Same as in Figure 8 but for t_2 = 1.5 ps. Again, AFSSH does reasonably well; the accuracy does not seem to degrade for longer t_2 times.

Second, turning to the cumulant expansion approach, we find that the latter is in good agreement with the exact results at t_2 = 0. Nevertheless, because the method does not capture nonadiabatic dynamics, this approach fails to capture the overall movement of peak intensity (from diagonal to off-diagonal) for longer t_2 times.

A more detailed comparison of the various components of the 2D spectra (GSB, SE, and ESA) is provided in Figure 8 for t_2 = 0 and in Figure 9 for t_2 = 1.5 ps. These components are the sum of the rephasing and nonrephasing components. For the most part, we find that AFSSH qualitatively matches these components individually, although there is clearly a negative feature of the electronic absorption signal (at t_2 = 0) that we cannot capture. Perhaps most importantly, our data do not lose much accuracy for longer t_2 times. That being said, although we do not show the data here, out method certainly does not capture rephasing and nonrephasing components individually; this distinction would be almost impossible given our ad-hoc treatment of the dynamics during the t_1 and t_3 times. After all, the distinction between rephasing and nonrephasing signals is the sign of the phase that is accumulated during the t_1 coherence time (see Figure 3).

Finally, in Figure 10, we consider the individual peak intensities for the overall spectra in Figure 7. Here, these peak intensities are computed as the signal strengths at fixed frequencies (−270 and +270 cm^{-1}) for the diagonal (part a) and off-diagonal (part b). The surface hopping method is in qualitative agreement with the rate of decay of the diagonal peaks, as well as the growth of the off-diagonal peak. This agreement is extremely encouraging, especially since, as described above, our method specifically ignores the delicate interplay between population dynamics and coherence dynamics. We note that Tempelaar and Reichman have also found very encouraging results using such an ansatz, although their approach was certainly more sophisticated than ours.

5. DISCUSSION AND CONCLUSIONS

In conclusion, we have presented a highly efficient approach to compute 2D spectra. Our method relies on evolving the dynamics over only the t_2 time period, and not during the t_1 and t_3 time periods. This drastic approximation cuts down the computational time significantly. For example, for the

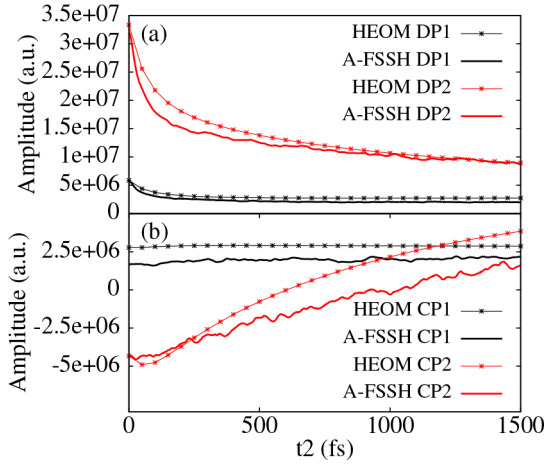


Figure 10. Comparison of (a) diagonal peaks (DP) and (b) cross peaks (CP) computed using AFSSH and HEOM. Note that AFSSH is able to recover the decay and rise of peaks and cross-peaks qualitatively.

calculations in Figure 10, with only 750 nuclear time steps (2 fs/step × 750 = 1.5 ps), converged surface hopping results required 15 min, as compared with about 1.5 h using the HEOM algorithm (which propagates t_1, t_2, and t_3 dynamics). For longer t_2 waiting times and/or more electronic states, the computational advantage of surface hopping should become even more apparent: after all, unlike HEOM, the memory requirements of surface hopping scale linearly with time and usually quadratically with the increasing number of electronic states. More importantly, HEOM is limited to model Hamiltonians with harmonic baths, whereas surface hopping can be applied to arbitrary, including *ab initio*, Hamiltonians.

Overall, the focus of our work is to capture the amount of homogeneous broadening and nonadiabatic population transfer between excited states as a function of t_2 for a 2D spectra. These features occur on important intrinsic time scales for a quantum subsystem in a classical environment, and accurate and efficient models to elucidate such time scales and predict accurate 2D spectra will necessarily have a large impact on many difficult experiments. Preliminary evidence provided above (as compared with HEOM) suggests that the current

DOI: 10.1021/acs.jpcb.8b08674
J. Phys. Chem. B XXXX, XXX, XXX−XXX

algorithm can achieve these goals if we operate under the assumptions of (a) dynamics in the inhomogeneous limit, (b) insignificant nonadiabatic transfer of population during the t_1 and t_3 coherence times, and (c) a high bath temperature, which are reasonable assumptions for most 2D experimental electronic spectra extracted from molecules in polar and/or hydrogen bonding solvents. In such cases, our results are in excellent agreement with the HEOM results. Furthermore, we accurately obtain not only the full spectra but also the individual components (GSB, SE, and ESA). That being said, we cannot capture the rephasing and nonrephasing components individually.

Looking forward, there are many future avenues for research to pursue:

- As developed, the current method is applicable only the inhomogeneous regime, with a slow bath. One would like to find a similar approach, if possible, for treating the case of a faster bath. Can a surface hopping approach be competitive with a cumulant approach in this regime?
- The approach presented above requires that we calculate the off-diagonal broadening parameter σ (see the text around eq 49). In section 3.4.1, we have offered one protocol for estimating σ by fitting a *diagonal* peak, as relevant for 2D-ES and 2D-IR spectra. For mixed, 2D-EV and 2D-VE spectra, the same approach should be valid if we simply fit an off-diagonal peak. This ansatz will be studied in the near future.
- As stipulated in section 3.2, the brute separation of coherences from populations is not very elegant and could almost certainly be improved. There is no unique means to calculate the conditional amplitudes $\rho_{lm}^{np}(t)$ *semiclassically*, and it is very possible that one can outperform the naive algorithm presented here, achieving improved accuracy with no substantial increase in computational cost.
- The cost of the present calculations is not very large, and given the capacity to run *ab initio* surface hopping trajectories nowadays,[57] we would like to calculate 2D spectra with *ab initio* accurate electronic structure that goes beyond the noninteracting model Frenkel system from section 2. In practice, such an application should not require much work at all. As far as the excited state dynamics are concerned, as with all surface hopping calculations, the only electronic structure information required are the excited state and ground state adiabatic energy surfaces and the nonadiabatic coupling vector, all of which are available with modern electronic structure packages. Thereafter, all that remains is to calculate the correlation function $g_{mn}(t)$ (which can be estimated classically with a simple *ground state* trajectory keeping track of energy gaps as in eq 89), build the $t_2 = 0$ ground-state bleach response functions S_2 and S_5 (using eqs 95, 98, 101, and 105), and fit the resulting real part of the sum in eq 49 so as to extract a broadening parameter σ. Note that, with this procedure, we would be sampling adiabatic (rather than excitonic) energy gaps for $g(t)$, but we believe that such a difference should not be meaningful as far as the final σ parameter is concerned; obviously, this ansatz must be tested.

In the end, calculating multidimensional spectra represents a very difficult but a very important challenge to dynamicists and electronic structure theorists. There would appear to be a great deal of room for new, semiclassical approaches in this burgeoning field, and we believe the method presented above should be a meaningful first step toward simulating *ab initio* 2D spectroscopy.

APPENDIX A. CUMULANT EXPANSION FOR COMPUTING THE SIGNALS IN EQS 31 AND 32

In this appendix, we give a reasonably comprehensive review of how one computes 2D spectra through a cumulant approximation.[47] We start with the derivation of the rephasing component of the ground state bleach (ϕ_2 in eq 23)

$$\phi_2(t_3,t_2,t_1) = \langle \mu_-(t_3+t_2+t_1)\, \mu_+(t_2+t_1)\, \rho(0)\, \mu_-(0)\, \mu_+(t_1)\rangle \tag{65}$$

$$= \langle \mu_-(\tau_3)\, \mu_+(\tau_2)\, \rho(0) \mu_-(0)\, \mu_+(\tau_1)\rangle \tag{66}$$

where

$$\tau_1 = t_1$$
$$\tau_2 = t_1 + t_2$$
$$\tau_3 = t_1 + t_2 + t_3 \tag{67}$$

Recall that we are working now in the excitonic (as opposed to site) basis, n, m below index eigenstates of H_{el} in eq 6. We ignore the off-diagonal nuclear−electronic coupling between excitonic states. Rather than calculate the correlation functions exactly by performing polaronic transformations and disentangling operators, we will take a simpler route and, given the Condon approximation and a bath of harmonic oscillators, we rewrite eq 13

$$\mu_+(t) = \mu_1^0 d_1^\dagger(t) + \mu_2^0 d_2^\dagger(t) \tag{68}$$

$$= \mu_1^0 d_1^\dagger e^{-iH_g t/\hbar} e^{iH_1 t/\hbar} + \mu_2^0 d_2^\dagger e^{-iH_g t/\hbar} e^{iH_2 t/\hbar} \tag{69}$$

$$\approx \mu_1^0 d_1^\dagger \exp\left(\int_0^t \frac{i}{\hbar}\tilde{\Omega}_1(t')\, dt'\right) + \mu_2^0 d_2^\dagger \exp\left(\int_0^t \frac{i}{\hbar}\tilde{\Omega}_2(t')\, dt'\right) \tag{70}$$

Here, H_g is the Hamiltonian for the ground state, and H_1/H_2 are the Hamiltonians that appear alongside excitonic states 1 and 2 along the diagonal. If the site (i) to adiabatic (m) transformation matrix is denoted U_{im}, then (using the notation of section 2),

$$H_m = H_b + \tilde{\epsilon}_m + \sum_{i=1}^{2}\sum_{\alpha=1}^{N} U_{im}^2 c_{i\alpha} R_{i\alpha} \tag{71}$$

With this notation, $\tilde{\Omega}_m$ is the energy gap for the exciton m, $\tilde{\Omega}_m = H_m - H_g$. Similarly

$$\mu_-(t) = \mu_1^0 d_1 e^{iH_1 t/\hbar} e^{-iH_g t/\hbar} + \mu_2^0 d_2 e^{iH_2 t/\hbar} e^{-iH_g t/\hbar} \tag{72}$$

$$\approx \mu_1^0 d_1 \exp\left(\int_0^t -\frac{i}{\hbar}\tilde{\Omega}_1(t')\, dt'\right) + \mu_2^0 d_2 \exp\left(\int_0^t -\frac{i}{\hbar}\tilde{\Omega}_2(t')\, dt'\right) \tag{73}$$

Equations 70 and 73 are the key approximations allowing for the cumulant approximation of 2D spectra, and it is worthwhile to explore the origins of these equations in details. First, we note that eqs 70 and 73 are exact provided that one performs all dynamics quantum mechanically and evaluates all exponential operators in a time-ordered fashion.[9] In other

DOI: 10.1021/acs.jpcb.8b08674
J. Phys. Chem. B XXXX, XXX, XXX−XXX

words, using simple arguments in the interaction picture, one can easily show that, for any two Hamiltonians H_a and H_b,

$$e^{iH_a t}e^{-iH_b t} = \mathcal{T}e^{\int i(H_a^I(t')-H_b^I(t'))\,dt'} \tag{74}$$

where the notation H_b^I denotes the Hamiltonian H_b in the interaction picture with $H_0 = H_a$: $H_b^I(t) \equiv e^{iH_a t}H_b e^{-iH_a t}$, $H_a^I(t) \equiv e^{iH_a t}H_a e^{-iH_a t} = H_a$. $\mathcal{T}$ represents time ordering.

Second, and more generally, for shifted harmonic oscillators, eqs 70 and 73 have a very intuitive meaning that can be seen by considering a polaronic transformation. Consider two shifted, one-dimensional harmonic oscillator Hamiltonians:

$$H_a = \frac{p^2}{2m} + \frac{1}{2}m\omega^2 x^2 \tag{75}$$

$$H_b = \frac{p^2}{2m} + \frac{1}{2}m\omega^2 (x-\lambda)^2 \tag{76}$$

Obviously, $H_b = UH_aU^\dagger$ with $U = e^{-i\lambda p/\hbar}$. Therefore, one can perform a few mathematical manipulations and show

$$e^{iH_a t/\hbar}e^{-iH_b t/\hbar} = e^{iH_a t}Ue^{-iH_a t}U^\dagger \tag{77}$$

$$= e^{iH_a t/\hbar}e^{-i\lambda p/\hbar}e^{-iH_a t}e^{i\lambda p/\hbar} \tag{78}$$

$$= e^{-i\lambda p^I(t)/\hbar}e^{i\lambda p/\hbar} \tag{79}$$

$$= e^{i\lambda(p-p^I(t))/\hbar}e^{i\phi(t)} \tag{80}$$

where $\phi = \frac{-\lambda}{2\hbar}[p^I(t),p]$. The last identity is effectively equivalent to the Campbell–Baker–Hausdorff principle and can be proven in many ways.[58] Thus, from eq 80, we find that eqs 70 and 73 effectively make the assumption that we will ignore the phase $e^{i\phi}$.

Third and finally, within the context of spectroscopy, we note also that the linear absorption spectrum between surfaces a and b arises from the Fourier transform of $\langle e^{iH_a t}e^{-iH_b t}\rangle$, where the average $\langle\ \rangle$ denotes a thermal, ground state average. Using eq 80, combined with Bloch's theorem for the expectation values of an exponentiated operator A that is linear in a and $a^\dagger$ (stating that $\langle e^A\rangle = e^{\langle A^2\rangle/2}$), one can show that

$$\langle e^{iH_a t}e^{-iH_b t}\rangle = e^{-\lambda^2(p-p^I(t))^2/2\hbar^2}e^{i\phi(t)} \tag{81}$$

By comparing this expression with the standard semiclassical Kubo expansion for the absorption spectrum in terms of the energy gap $H_{ba} \equiv H_b - H_a$,[58] one can show that the approximations underlying eqs 70 and 73 (i.e., ignoring the phase $e^{i\phi}$ in eq 80) are equivalent to ignoring the imaginary part of the frequency–frequency correlation function $\langle \delta H_{ba}^I(t)\delta H_{ba}^I\rangle$. Here, $\delta H_{ba} \equiv H_{ba} - \langle H_{ba}\rangle$.

Returning to the semiclassical calculation, next we substitute eqs 70 and 73 into eq 65, and find

$$\begin{aligned}\phi_2(t_3,t_2,t_1) = \Bigg\langle &\left(\mu_1^0 d_1 \exp\left(\int_0^{\tau_3} -\frac{i}{\hbar}\tilde{\Omega}_1(t')\,dt'\right) + \mu_2^0 d_2 \exp\left(\int_0^{\tau_3} -\frac{i}{\hbar}\tilde{\Omega}_2(t')\,dt'\right)\right)\\ &\times\left(\mu_1^0 d_1^\dagger \exp\left(\int_0^{\tau_2} \frac{i}{\hbar}\tilde{\Omega}_1(t')\,dt'\right) + \mu_2^0 d_2^\dagger \exp\left(\int_0^{\tau_2} \frac{i}{\hbar}\tilde{\Omega}_2(t')\,dt'\right)\right)\\ &\times\rho(0)(\mu_1^0 d_1 + \mu_2^0 d_2)\\ &\times\left(\mu_1^0 d_1^\dagger \exp\left(\int_0^{\tau_1} \frac{i}{\hbar}\tilde{\Omega}_1(t')\,dt'\right) + \mu_2^0 d_2^\dagger \exp\left(\int_0^{\tau_1} \frac{i}{\hbar}\tilde{\Omega}_2(t')\,dt'\right)\right)\Bigg\rangle\end{aligned} \tag{82}$$

Since $\rho(0) = |g\rangle\langle g|$, out of the 16 terms in eq 82, only four terms are nonzero (assuming no nonadiabatic dynamics)

$$\phi_2(t_3,t_2,t_1) = \sum_{m=1}^{2}\sum_{n=1}^{2}\kappa_{mn} \tag{83}$$

with

$$\kappa_{mn} = \mu_m^{0^2}\mu_n^{0^2}\left\langle \exp\left(\int_0^{\tau_1}\frac{i}{\hbar}\tilde{\Omega}_m(t')\,dt' + \int_0^{\tau_2}\frac{i}{\hbar}\tilde{\Omega}_n(t')\,dt' - \int_0^{\tau_3}\frac{i}{\hbar}\tilde{\Omega}_n(t')\,dt'\right)\right\rangle \tag{84}$$

In proceeding from eq 82 to eq 84, we are again approximating that, for harmonic oscillator operators A and B that are linear in a and $a^\dagger$, we have $\langle e^A e^B\rangle \approx \langle e^{A+B}\rangle$ (just as we did when we moved from eq 79 to eq 80 and ignored the phase $e^{i\phi}$).

At this point, we follow the standard formulation of the cumulant expansion, and we separate fluctuations from averages:

$$\tilde{\Omega}_m(t) = \langle\tilde{\Omega}_m\rangle + \delta\tilde{\Omega}_m(t) \tag{85}$$

$$\equiv \tilde{\epsilon}_m + \delta\tilde{\Omega}_m(t) \tag{86}$$

We then substitute eq 86 into eq 84. We find

$$\kappa_{mn} = \mu_m^{0^2}\mu_n^{0^2}e^{i\tilde{\epsilon}_m t_1/\hbar}e^{-i\tilde{\epsilon}_n t_3/\hbar}\left\langle \exp\left(\int_0^{\tau_1}\frac{i}{\hbar}\delta\tilde{\Omega}_m(t')\,dt' + \int_0^{\tau_2}\frac{i}{\hbar}\delta\tilde{\Omega}_n(t')\,dt' - \int_0^{\tau_3}\frac{i}{\hbar}\delta\tilde{\Omega}_n(t')\,dt'\right)\right\rangle \tag{87}$$

And if we further expand eq 87 to second order (the first order is zero) and approximate the effect of time ordering as introducing a factor of 1/2 in eqs 89 and 90,[59] we find

$$\kappa_{mn} = \mu_m^{0^2}\mu_n^{0^2}e^{i\tilde{\epsilon}_m t_1/\hbar}e^{-i\tilde{\epsilon}_n t_3/\hbar}(1 - g_{mm}(\tau_1) - g_{nn}(\tau_2) - g_{nn}(\tau_3) - h_{mn}(\tau_1,\tau_2) + h_{mn}(\tau_1,\tau_3) + h_{nn}(\tau_2,\tau_3)) \tag{88}$$

where

$$g_{mn}(\tau) = \frac{1}{2\hbar^2}\int_0^\tau dt'\int_0^\tau dt''\,\langle\delta\tilde{\Omega}_m(t')\,\delta\tilde{\Omega}_n(t'')\rangle \tag{89}$$

$$h_{mn}(\tau_1,\tau_2) = \frac{1}{\hbar^2}\int_0^{\tau_1} dt'\int_0^{\tau_2} dt''\,\langle\delta\tilde{\Omega}_m(t')\,\delta\tilde{\Omega}_n(t'')\rangle \tag{90}$$

Henceforward, these expectation values will be evaluated as real, classical equilibrium correlation functions, with classical time reversal symmetry, so that $\langle\delta\tilde{\Omega}_m(t')\,\delta\tilde{\Omega}_n(t'')\rangle = \langle\delta\tilde{\Omega}_m(t'')\,\delta\tilde{\Omega}_n(t')\rangle$ and therefore $h_{mn}(\tau_1,\tau_2) = h_{mn}(\tau_2,\tau_1)$. With this approximation, one can easily show that there is a simple relationship between h_{mn} and g_{mn}, namely

$$h_{mn}(\tau_1,\tau_2) = g_{mn}(\tau_1) + g_{mn}(\tau_2) - g_{mn}(|\tau_1 - \tau_2|) \tag{91}$$

Finally, if we substitute eq 91 into eq 88, and use eq 67, we recover

DOI: 10.1021/acs.jpcb.8b08674
J. Phys. Chem. B XXXX, XXX, XXX−XXX

$$\kappa_{mn} = {\mu_m^0}^2 {\mu_n^0}^2 e^{i\tilde{\epsilon}_m t_1/\hbar} e^{-i\tilde{\epsilon}_n t_3/\hbar} (1 - g_{mm}(t_1) + g_{mn}(t_2) - g_{nn}(t_3) - g_{mn}(t_1+t_2) - g_{mn}(t_2+t_3) + g_{mn}(t_1+t_2+t_3)) \quad (92)$$

$$\approx {\mu_m^0}^2 {\mu_n^0}^2 e^{i\tilde{\epsilon}_m t_1/\hbar} e^{-i\tilde{\epsilon}_n t_3/\hbar} e^{-N_2^{mn}} \quad (93)$$

At this point, we have a complete expression for the rephasing component of the ground-state bleach ϕ_2.

If we now follow the same steps for all of the diagrams in eqs 22−27, we obtain

$$S_1(\omega_1, t_2, \omega_3) = \sum_{m=1}^{2}\sum_{n=1}^{2} {\tilde{\mu}_m}^2 {\tilde{\mu}_n}^2 \int_0^\infty dt_1 \times \int_0^\infty dt_3 \cos((\omega_1-\tilde{\epsilon}_m)t_1-(\omega_3-\tilde{\epsilon}_n)t_3+(\tilde{\epsilon}_n-\tilde{\epsilon}_m)t_2) \exp(-N_1^{mn}) \quad (94)$$

$$S_2(\omega_1,t_2,\omega_3) = \sum_{m=1}^{2}\sum_{n=1}^{2} {\tilde{\mu}_m}^2 {\tilde{\mu}_n}^2 \int_0^\infty dt_1 \times \int_0^\infty dt_3 \cos((\omega_1-\tilde{\epsilon}_m)t_1-(\omega_3-\tilde{\epsilon}_n)t_3) \exp(-N_2^{mn}) \quad (95)$$

$$S_3(\omega_1,t_2,\omega_3) = \sum_{m=1}^{2} {\tilde{\mu}_m}^2 {\tilde{\mu}_{m'}}^2 \int_0^\infty dt_1 \times \int_0^\infty dt_3 \cos((\omega_1-\tilde{\epsilon}_m)t_1-(\omega_3-\tilde{\epsilon}_{m'})t_3) \exp(-N_{3a}^{mm'}) + \sum_{m=1}^{2} {\tilde{\mu}_m}^2 {\tilde{\mu}_{m'}}^2 \int_0^\infty dt_1 \times \int_0^\infty dt_3 \cos((\omega_1-\tilde{\epsilon}_m)t_1-(\omega_3-\tilde{\epsilon}_{m'})t_3+(\tilde{\epsilon}_n-\tilde{\epsilon}_m)t_2) \exp(-N_{3b}^{mm'}) \quad (96)$$

$$S_4(\omega_1,t_2,\omega_3) = \sum_{m=1}^{2}\sum_{n=1}^{2} {\tilde{\mu}_m}^2 {\tilde{\mu}_n}^2 \int_0^\infty dt_1 \times \int_0^\infty dt_3 \cos((\omega_1-\tilde{\epsilon}_m)t_1+(\omega_3-\tilde{\epsilon}_m)t_3+(\tilde{\epsilon}_n-\tilde{\epsilon}_m)t_2) \exp(-N_4^{mn}) \quad (97)$$

$$S_5(\omega_1,t_2,\omega_3) = \sum_{m=1}^{2}\sum_{n=1}^{2} {\tilde{\mu}_m}^2 {\tilde{\mu}_n}^2 \int_0^\infty dt_1 \times \int_0^\infty dt_3 \cos((\omega_1-\tilde{\epsilon}_m)t_1+(\omega_3-\tilde{\epsilon}_n)t_3) \exp(-N_5^{mn}) \quad (98)$$

$$S_6(\omega_1,t_2,\omega_3) = \sum_{m=1}^{2} {\tilde{\mu}_m}^2 {\tilde{\mu}_{m'}}^2 \int_0^\infty dt_1 \times \int_0^\infty dt_3 \cos((\omega_1-\tilde{\epsilon}_m)t_1+(\omega_3-\tilde{\epsilon}_{m'})t_3) \exp(-N_{6a}^{mn}) + \sum_{m=1}^{2} {\tilde{\mu}_m}^2 {\tilde{\mu}_{m'}}^2 \int_0^\infty dt_1 \times \int_0^\infty dt_3 \cos((\omega_1-\tilde{\epsilon}_m)t_1+(\omega_3-\tilde{\epsilon}_m)t_3+(\tilde{\epsilon}_n-\tilde{\epsilon}_m)t_2) \exp(-N_{6b}^{mm'}) \quad (99)$$

where $\tilde{\mu}_i$ and $\tilde{\epsilon}_i$ are the dipole moments and the excitation energies in the excitonic basis. The notation m' signifies the other single particle excitonic state other than m; e.g., m' is 2 if m = 1, and m' is 1 if m = 2. The noises N_i are given by

$$N_1^{m,n} = g_{mn}(t_1) - g_{mn}(t_2) + g_{mn}(t_3) + g_{mm}(t_1+t_2) + g_{nn}(t_2+t_3) - g_{mn}(t_1+t_2+t_3) \quad (100)$$

$$N_2^{m,n} = g_{mm}(t_1) - g_{mn}(t_2) + g_{nn}(t_3) + g_{mn}(t_1+t_2) + g_{mn}(t_2+t_3) - g_{mn}(t_1+t_2+t_3) \quad (101)$$

$$N_{3a}^{m,m'} = g_{mm}(t_1) - g_{mm'}(t_2) + g_{m'm'}(t_3) + g_{mm'}(t_1+t_2) + g_{mm'}(t_2+t_3) - g_{mm'}(t_1+t_2+t_3) \quad (102)$$

$$N_{3b}^{m,m'} = g_{mm'}(t_1) - g_{mm'}(t_2) + g_{mm'}(t_3) + g_{mm}(t_1+t_2) + g_{m'm'}(t_2+t_3) - g_{mm'}(t_1+t_2+t_3) \quad (103)$$

$$N_4^{m,n} = g_{mn}(t_1) + g_{nn}(t_2) + g_{mn}(t_3) - g_{mn}(t_1+t_2) - g_{mn}(t_2+t_3) + g_{mm}(t_1+t_2+t_3) \quad (104)$$

$$N_5^{m,n} = g_{mm}(t_1) + g_{mn}(t_2) + g_{nn}(t_3) - g_{mn}(t_1+t_2) - g_{mn}(t_2+t_3) + g_{mn}(t_1+t_2+t_3) \quad (105)$$

$$N_{6a}^{m,m'} = g_{mm}(t_1) + g_{mm'}(t_2) + g_{m'm'}(t_3) - g_{mm'}(t_1+t_2) - g_{mm'}(t_2+t_3) + g_{mm'}(t_1+t_2+t_3) \quad (106)$$

$$N_{6b}^{m,m'} = g_{mm'}(t_1) + g_{m'm'}(t_2) + g_{mm'}(t_3) - g_{mm'}(t_1+t_2) - g_{mm'}(t_2+t_3) + g_{mm}(t_1+t_2+t_3) \quad (107)$$

APPENDIX B. DERIVATION OF EQ 34

We start with a simple Hamiltonian—a two level system coupled to a harmonic bath:

$$H = H_1 + H_2 \quad (108)$$

$$H_1 = \sum_{n=1}^{N} \frac{{p_n}^2}{2m} + \frac{1}{2} m {\omega_n}^2 {R_n}^2 \quad (109)$$

$$H_2 = H_1 + \sum_{n=1}^{N} c_n R_n + \epsilon \quad (110)$$

with the couplings c_n given by the Drude spectral density defined in eqs 9 and 10.

The autocorrelation function in eq 34 is given by

$$\langle \delta\Omega(t)\, \delta\Omega(0)\rangle = \left\langle \sum_{n=1}^{N} c_n R_n(t) \sum_{m=1}^{N} c_m R_m(0) \right\rangle \quad (111)$$

$$= \left\langle \sum_{n=1}^{N} {c_n}^2 R_n(t)\, R_n(0) \right\rangle \quad (112)$$

Here, we have assumed that the bath modes are independent. We will now further assume entirely classical motion so that, for a harmonic oscillator, $R_n(t) = R_n(0)\cos(\omega_n t) + \frac{p_n}{m\omega_n}\sin(\omega_n t)$. Inserting these dynamics into eq 112, and using classical thermal equilibrium,

DOI: 10.1021/acs.jpcb.8b08674
J. Phys. Chem. B XXXX, XXX, XXX−XXX

$$\langle R_n(0)^2 \rangle = \frac{k_B T}{m\omega_n^2} \tag{113}$$

we find

$$\langle \delta\Omega(t)\, \delta\Omega(0) \rangle = \sum_{n=1}^{N} k_B T \frac{c_n^2}{m\omega_n^2} \cos(\omega_n t) \tag{114}$$

$$= k_B T \frac{2}{\pi} \int_0^\infty d\omega\, \frac{J(\omega)}{\omega} \cos(\omega t) \tag{115}$$

$$= 4 k_B T V_r \frac{1}{\pi} \int_0^\infty d\omega\, \frac{\gamma \cos(\omega t)}{\omega^2 + \gamma^2} \tag{116}$$

$$= 2 k_B T V_r e^{-\gamma t} \tag{117}$$

For the last step, we have computed the Fourier transform of a Lorentzian

$$\frac{1}{\pi} \int_{-\infty}^{\infty} d\omega\, e^{i\omega t} \frac{\Gamma}{\omega^2 + \Gamma^2} = e^{-\Gamma t} \tag{118}$$

Comparing eq 117 with eq 34 gives $\Delta = \sqrt{2 k_B T V_r}$ and $\tau_c = 1/\gamma$.

AUTHOR INFORMATION

Corresponding Authors

*E-mail: amberj@chem.iitb.ac.in.

*E-mail: subotnik@sas.upenn.edu.

ORCID

Amber Jain: 0000-0002-8003-8716

Jessica M. Anna: 0000-0001-5440-6987

Notes

The authors declare no competing financial interest.

ACKNOWLEDGMENTS

J.E.S. acknowledges funding from the US Air Force Office of Scientific Research (USAFOSR), AFOSR FA9550-18-1-0497. A.J. acknowledges a seed grant from the Indian Institute of Technology Bombay for the generous support. A.S.P. acknowledges startup funding from California State University, Fullerton, as well as computational support from the Center for Computational and Applied Mathematics. J.M.A. acknowledges support from the U.S. Department of Energy, Office of Science, Office of Basic Energy Sciences under award number DE-SC-0016043.

REFERENCES

(1) Hybl, J. D.; Albrecht, A. W.; Faeder, S. M. G.; Jonas, D. M. Two-dimensional electronic spectroscopy. *Chem. Phys. Lett.* **1998**, *297*, 307−313.

(2) Gallagher, S. M.; Albrecht, A. W.; Hybl, J. D.; Landin, B. L.; Rajaram, B.; Jonas, D. M. Heterodyne detection of the complete electric field of femtosecond four-wave mixing signals. *J. Opt. Soc. Am. B* **1998**, *15*, 2338−2345.

(3) Hybl, J. D.; Ferro, A. A.; Jonas, D. M. Two-dimensional Fourier transform electronic spectroscopy. *J. Chem. Phys.* **2001**, *115*, 6606−6622.

(4) Hybl, J. D.; Yu, A.; Farrow, D. A.; Jonas, D. M. Polar Solvation Dynamics in the Femtosecond Evolution of Two-Dimensional Fourier Transform Spectra. *J. Phys. Chem. A* **2002**, *106*, 7651−7654.

(5) Brixner, T.; Stenger, J.; Vaswani, H. M.; Cho, M.; Blankenship, R. E.; Fleming, G. R. Two-dimensional spectroscopy of electronic couplings in photosynthesis. *Nature* **2005**, *434*, 625.

(6) Mukamel, S. Multidimensional femtosecond correlation spectroscopies of electronic and vibrational excitations. *Annu. Rev. Phys. Chem.* **2000**, *51*, 691−729.

(7) Jonas, D. M. Two-Dimensional Femtosecond Spectroscopy. *Annu. Rev. Phys. Chem.* **2003**, *54*, 425−463.

(8) Cho, M. Coherent Two-Dimensional Optical Spectroscopy. *Chem. Rev.* **2008**, *108*, 1331−1418.

(9) Tokmakoff, A. *Time-Dependent Quantum Mechanics and Spectroscopy*; http://tdqms.uchicago.edu/page/tdqms-notes.

(10) Khalil, M.; Demirdöven, N.; Tokmakoff, A. Coherent 2D IR Spectroscopy: Molecular Structure and Dynamics in Solution. *J. Phys. Chem. A* **2003**, *107*, 5258−5279.

(11) Gaynor, J. D.; Courtney, T. L.; Balasubramanian, M.; Khalil, M. Fourier transform two-dimensional electronic-vibrational spectroscopy using an octave-spanning mid-IR probe. *Opt. Lett.* **2016**, *41*, 2895−2898.

(12) Kubo, R. A stochastic theory of line shape. *Adv. Chem. Phys.* **2007**, *15*, 101−127.

(13) Saven, J. G.; Skinner, J. L. A molecular theory of the line shape: Inhomogeneous and homogeneous electronic spectra of dilute chromophores in nonpolar fluids. *J. Chem. Phys.* **1993**, *99*, 4391−4402.

(14) Skinner, J. L. Vibrational line shapes and spectral diffusion in fluids. *Mol. Phys.* **2008**, *106*, 2245−2253.

(15) Sun, X.; Geva, E. Equilibrium Fermi's Golden Rule Charge Transfer Rate Constants in the Condensed Phase: The Linearized Semiclassical Method vs Classical Marcus Theory. *J. Phys. Chem. A* **2016**, *120*, 2976−2990.

(16) Fried, L. E.; Mukamel, S. Nonlinear Electronic Spectroscopy in Condensed Phases. *Adv. Chem. Phys.* **2007**, *84*, 435−516.

(17) Shemetulskis, N. E.; Loring, R. F. Semiclassical theory of the photon echo: Applications to polar fluids. *J. Chem. Phys.* **1992**, *97*, 1217−1225.

(18) Kapral, R.; Ciccotti, G. Mixed quantum-classical dynamics. *J. Chem. Phys.* **1999**, *110*, 8919−8929.

(19) Sulc, M.; Hernandez, H.; Martinez, T. J.; Vanicek, J. Relation of exact Gaussian basis methods to the dephasing representation: Theory and application to time-resolved electronic spectra. *J. Chem. Phys.* **2013**, *139*, 034112.

(20) Zimmermann, T.; Vanicek, J. Efficient on-the-fly ab initio semiclassical method for computing time-resolved nonadiabatic electronic spectra with surface hopping or Ehrenfest dynamics. *J. Chem. Phys.* **2014**, *141*, 134102.

(21) Crespo-Otero, R.; Barbatti, M. Recent Advances and Perspectives on Nonadiabatic Mixed Quantum−Classical Dynamics. *Chem. Rev.* **2018**, *118*, 7026−7068.

(22) Petit, A. S.; Subotnik, J. E. Calculating time-resolved differential absorbance spectra for ultrafast pump-probe experiments with surface hopping trajectories. *J. Chem. Phys.* **2014**, *141*, 154108.

(23) Crespo-Otero, R.; Barbatti, M. Spectrum simulation and decomposition with nuclear ensemble: formal derivation and application to benzene, furan and 2-phenylfuran. *Theor. Chem. Acc.* **2012**, *131*, 1237.

(24) Daku, L. M. L.; Linares, J.; Boillot, M.-L. Ab initio static and molecular dynamics study of the absorption spectra of the 4-styrylpyridine photoswitch in its cis and trans forms. *Phys. Chem. Chem. Phys.* **2010**, *12*, 6107−6123.

(25) Ben-Nun, M.; Martinez, T. J. Ab initio quantum molecular dynamics. *Adv. Chem. Phys.* **2002**, *121*, 439−512.

(26) Segatta, F.; Cupellini, L.; Jurinovich, S.; Mukamel, S.; Dapor, M.; Taioli, S.; Garavelli, M.; Mennucci, B. A Quantum Chemical Interpretation of Two-Dimensional Electronic Spectroscopy of Light-Harvesting Complexes. *J. Am. Chem. Soc.* **2017**, *139*, 7558−7567.

(27) Makri, N.; Makarov, D. E. Tensor propagator for iterative quantum time evolution of reduced density matrices. I. Theory. *J. Chem. Phys.* **1995**, *102*, 4600−4610.

(28) Makri, N.; Makarov, D. E. Tensor propagator for iterative quantum time evolution of reduced density matrices. II. Numerical methodology. *J. Chem. Phys.* **1995**, *102*, 4611−4618.

DOI: 10.1021/acs.jpcb.8b08674
J. Phys. Chem. B XXXX, XXX, XXX−XXX

(29) Makri, N. Numerical path integral techniques for long time dynamics of quantum dissipative systems. *J. Math. Phys.* **1995**, *36*, 2430−2457.
(30) Chen, L.; Zheng, R.; Shi, Q.; Yan, Y. Optical line shapes of molecular aggregates: Hierarchical equations of motion method. *J. Chem. Phys.* **2009**, *131*, 094502.
(31) Chen, L.; Zheng, R.; Shi, Q.; Yan, Y. Two-dimensional electronic spectra from the hierarchical equations of motion method: Application to model dimers. *J. Chem. Phys.* **2010**, *132*, 024505.
(32) Shi, Q.; Geva, E. A comparison between different semiclassical approximations for optical response functions in nonpolar liquid solution. II. The signature of excited state dynamics on two-dimensional spectra. *J. Chem. Phys.* **2008**, *129*, 124505.
(33) Schmidt, J.; Roberts, S.; Loparo, J.; Tokmakoff, A.; Fayer, M.; Skinner, J. Are water simulation models consistent with steady-state and ultrafast vibrational spectroscopy experiments? *Chem. Phys.* **2007**, *341*, 143−157.
(34) Auer, B.; Kumar, R.; Schmidt, J.; Skinner, J. Hydrogen bonding and Raman, IR, and 2D-IR spectroscopy of dilute HOD in liquid D2O. *Proc. Natl. Acad. Sci. U. S. A.* **2007**, *104*, 14215−14220.
(35) Yan, Y. J.; Mukamel, S. Photon echoes of polyatomic molecules in condensed phases. *J. Chem. Phys.* **1991**, *94*, 179−190.
(36) Sung, J.; Silbey, R. J. Four wave mixing spectroscopy for a multilevel system. *J. Chem. Phys.* **2001**, *115*, 9266−9287.
(37) Asbury, J. B.; Steinel, T.; Stromberg, C.; Corcelli, S.; Lawrence, C.; Skinner, J.; Fayer, M. Water dynamics: Vibrational echo correlation spectroscopy and comparison to molecular dynamics simulations. *J. Phys. Chem. A* **2004**, *108*, 1107−1119.
(38) Loring, R. F. Mean-trajectory approximation for electronic and vibrational-electronic nonlinear spectroscopy. *J. Chem. Phys.* **2017**, *146*, 144106.
(39) Meyer, H. D.; Miller, W. H. Analysis and extension of some recently proposed classical models for electronic degrees of freedom. *J. Chem. Phys.* **1980**, *72*, 2272.
(40) Stock, G.; Thoss, M. Semiclassical Description of Nonadiabatic Quantum Dynamics. *Phys. Rev. Lett.* **1997**, *78*, 578.
(41) Ramesh, P.; Loring, R. F. Thermal Population Fluctuations in Two-Dimensional Infrared Spectroscopy Captured with Semiclassical Mechanics. *J. Phys. Chem. B* **2018**, *122*, 3647−3654.
(42) Provazza, J.; Segatta, F.; Garavelli, M.; Coker, D. F. Semiclassical Path Integral Calculation of Nonlinear Optical Spectroscopy. *J. Chem. Theory Comput.* **2018**, *14*, 856.
(43) van der Vegte, C. P.; Dijkstra, A. G.; Knoester, J.; Jansen, T. L. C. Calculating Two-Dimensional Spectra with the Mixed Quantum-Classical Ehrenfest Method. *J. Phys. Chem. A* **2013**, *117*, 5970−5980.
(44) Tempelaar, R.; Van der Vegte, C. P.; Knoester, J.; Jansen, T. L. Surface hopping modeling of two-dimensional spectra. *J. Chem. Phys.* **2013**, *138*, 164106.
(45) Tempelaar, R.; Reichman, D. R. Generalization of fewest-switches surface hopping for coherences. *J. Chem. Phys.* **2018**, *148*, 102309.
(46) Hamm, P.; Zanni, M. *Concepts and Methods of 2D Infrared Spectroscopy*, Cambridge University Press, 2011.
(47) Mukamel, S. *Principles of nonlinear optical spectroscopy*; Oxford series in optical and imaging sciences; Oxford University Press, 1995.
(48) It is fairly easy to show that, if $\{A_j\}$ are a set of Hermitian operators and ρ is a Hermitian density operator, $\mathrm{tr}(\rho[A_1,A_2])$ is imaginary, $\mathrm{tr}(\rho[[A_1,A_2],A_3])$ is real, $\mathrm{tr}(\rho[[[A_1,A_2],A_3],A_4])$ is imaginary, and so forth.
(49) To see this, suppose the electric field is made up of δ-function pulses at times $t = 0$, t_1', and $t_1' + t_2'$: $\mathbf{E}(t) = \mathbf{E}_1\delta(t) + \mathbf{E}_2\delta(t-t_1') + \mathbf{E}_2\delta(t-t_1'-t_2')$. Then, if we plug into eq 16, we easily find that $P(t) \propto R(t_3',t_2',t_1')$, where $t_3' = t - t_2' - t_1'$.
(50) Tanimura, Y.; Kubo, R. Time Evolution of a Quantum System in Contact with a Nearly Gaussian-Markovian Noise Bath. *J. Phys. Soc. Jpn.* **1989**, *58*, 101.
(51) Tanimura, Y. Reduced hierarchy equations of motion approach with Drude plus Brownian spectral distribution: Probing electron transfer processes by means of two-dimensional correlation spectroscopy. *J. Chem. Phys.* **2012**, *137*, 22A550.
(52) The adiabatic dipole moments, which depend on the nuclear geometry, must also be included in this averaging. See section 3.4.2 for a detailed description.
(53) Jain, A.; Alguire, E.; Subotnik, J. E. An Efficient, Augmented Surface Hopping Algorithm That Includes Decoherence for Use in Large-Scale Simulations. *J. Chem. Theory Comput.* **2016**, *12*, 5256−5268.
(54) Petit, A. S.; Subotnik, J. E. How to calculate linear absorption spectra with lifetime broadening using fewest switches surface hopping trajectories: a simple generalization of ground-state Kubo theory. *J. Chem. Phys.* **2014**, *141*, 014107.
(55) Petit, A. S.; Subotnik, J. E. Appraisal of Surface Hopping as a Tool for Modeling Condensed Phase Linear Absorption Spectra. *J. Chem. Theory Comput.* **2015**, *11*, 4328−4341.
(56) In this work, for the model Hamiltonian given by eqs 5−8, we use the parameters $\Delta = \sqrt{2V_r k_B T}$, and $\tau_c = 1/\gamma$.
(57) Medders, G. R.; Alguire, E. C.; Jain, A.; Subotnik, J. E. Ultrafast Electronic Relaxation through a Conical Intersection: Nonadiabatic Dynamics Disentangled through an Oscillator Strength-Based Diabatization Framework. *J. Phys. Chem. A* **2017**, *121*, 1425−1434.
(58) Nitzan, A. *Chemical Dynamics in Condensed Phases*; Oxford University Press, 2006.
(59) For absorption spectroscopy, one can recover the exact spectrum by calculating the frequency−frequency correlation functions exactly (i.e., quantum mechanically) and not ignoring time-ordering (i.e., using eq 33 instead of eq 89). See ref 9.

DOI: 10.1021/acs.jpcb.8b08674
J. Phys. Chem. B XXXX, XXX, XXX−XXX